ACS Chemical Neuroscience

pubs.acs.org/chemneuro
Research Article

Patient Brain Organoids Identify a Link between the 16p11.2 Copy Number Variant and the *RBFOX1* Gene

Milos Kostic,[§] Joseph J. Raymond,[§] Christophe A. C. Freyre, Beata Henry, Tayfun Tumkaya, Jivan Khlghatyan, Jill Dvornik, Jingyao Li, Jack S. Hsiao, Seon Hye Cheon, Jonathan Chung, Yishan Sun, Ricardo E. Dolmetsch, Kathleen A. Worringer, and Robert J. Ihry*

Cite This: *ACS Chem. Neurosci.* 2023, 14, 3993−4012

ABSTRACT: Copy number variants (CNVs) that delete or duplicate 30 genes within the 16p11.2 genomic region give rise to a range of neurodevelopmental phenotypes with high penetrance in humans. Despite the identification of this small region, the mechanisms by which 16p11.2 CNVs lead to disease are unclear. Relevant models, such as human cortical organoids (hCOs), are needed to understand the human-specific mechanisms of neurodevelopmental disease. We generated hCOs from 17 patients and controls, profiling 167,958 cells with single-cell RNA-sequencing analysis, which revealed neuronal-specific differential expression of genes outside the 16p11.2 region that are related to cell−cell adhesion, neuronal projection growth, and neurodevelopmental disorders. Furthermore, 16p11.2 deletion syndrome organoids exhibited reduced mRNA and protein levels of RBFOX1, a gene that can also harbor CNVs linked to neurodevelopmental phenotypes. We found that the genes previously shown to be regulated by RBFOX1 are also perturbed in organoids from patients with the 16p11.2 deletion syndrome and thus identified a novel link between independent CNVs associated with neuronal development and autism. Overall, this work suggests convergent signaling, which indicates the possibility of a common therapeutic mechanism across multiple rare neuronal diseases.

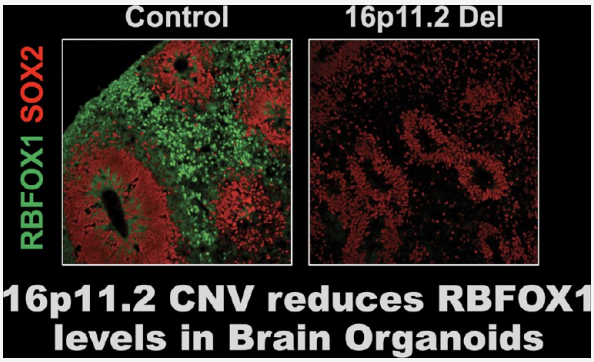

KEYWORDS: *brain organoids, CNV, 16p11.2, scRNA-seq, RBFOX1, autism*

INTRODUCTION

Copy number variants (CNVs) play a major role in the etiology of neuropsychiatric and neurodevelopmental disorders. A CNV may reside in a single gene, such as *RBFOX1*, which encodes a protein regulating mRNA alternative splicing in neurons and is located on chromosome 16p13.3.[1] *RBFOX1* CNVs are linked to autism spectrum disorder (ASD), intellectual disability (ID), and epilepsy.[1−4] A CNV may also span a specific chromosomal segment or cytogenetic band, such as 1q21.1, 7q11.23, 15q11.2, 16p11.2, 17q12, and 22q11.2 (chromosome number, p/q denotes the long/short arm of each chromosome, and band number), causing deletion or duplication of a whole set of resident genes.[5,6] The CNVs spanning chromosome 16p11.2 have been associated with multiple neuropsychiatric and neurodevelopmental disorders and are the focus of our current study.[7] Some clinical diagnoses or phenotypes are common to both 16p11.2 hemideletion (1 copy loss) and hemiduplication (1 copy gain), such as ASD, ID, and epilepsy.[7−14] Other diagnoses or phenotypes are unique to the actual copy number and can be reciprocal between hemideletion and hemiduplication. For example, 16p11.2 hemideletions are linked to macrocephaly and obesity, while hemiduplications are linked to microcephaly and low body mass index (BMI).[15,16] Furthermore, clinical phenotypes may also vary by the exact chromosomal breaking points of a 16p11.2 CNV. In humans, the most common genomic breakpoints (BPs) underlying either 16p11.2 hemideletion or hemiduplication are BP4-BP5, which straddle an ∼600 kilobase pair (kbp) centromere-proximal region of 16p11.2.[17,18] However, some individuals carry CNVs with BPs flanking a more distal region (e.g., BP1-BP3, BP2-BP3, and BP1-BP4) or flanking both proximal and distal regions (e.g., BP1-BP5). Interestingly, susceptibility to schizophrenia (SCZ) was only associated with proximal duplications and distal deletions, suggesting differential roles among resident genes and/or noncoding elements between the proximal and distal regions of 16p11.2 in human brain development and

Received: June 27, 2023
Accepted: September 14, 2023
Published: October 30, 2023

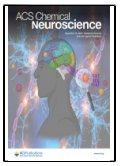

https://doi.org/10.1021/acschemneuro.3c00442
ACS Chem. Neurosci. 2023, 14, 3993−4012

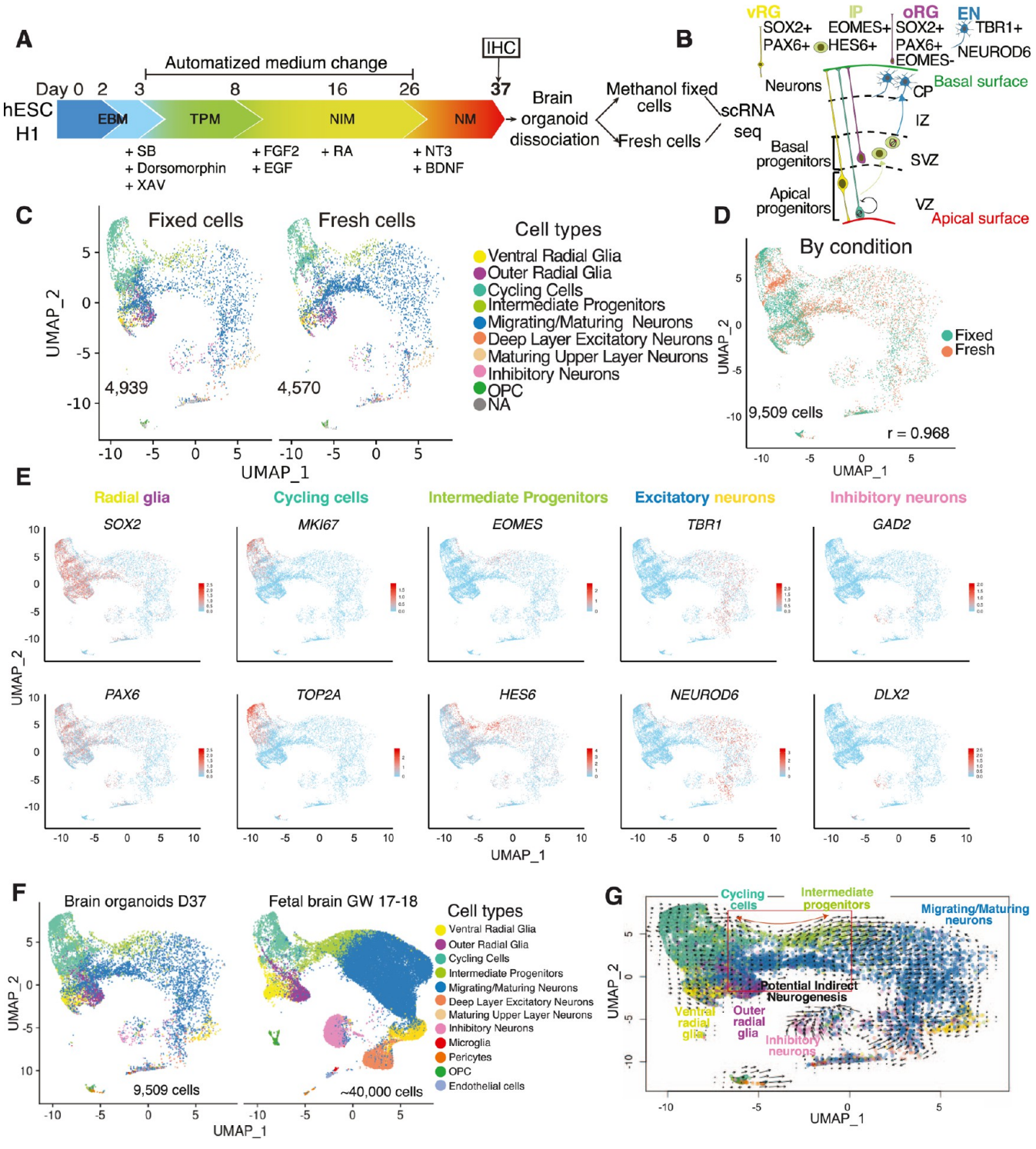

Figure 1. Semi-automated generation of hCOs yields crucial aspects of human neurogenesis. (A) Schematic of hCO differentiation and methanol fixation protocols for the cell line hESC-H1. (B) Schematic of neocortical development and its main cell types. (C) Uniform manifold approximation and projection (UMAP) embedding plot of 4939 methanol-fixed cells and 4570 fresh cells, 37 day old hCOs, with all identified cell types; sample of 20 hCOs (10 fresh and 10 fixed) and the cell line hESC-H1. (D) UMAP plot showing the overlap of methanol fixed and fresh cortical organoid cells, Pearson's correlation $r = 0.968$. (E) UMAP plots showing expression of canonical gene markers for main cell types, which were identified in fresh and fixed cells combined at day 37. (F) UMAP plot integration of hCOs (day 37, 9509 fixed and fresh cells) with fetal brain atlas (GW17−18, ~40,000 cells,[48]), a majority of hCO cells were allocated to the neuronal progenitor and immature identities; GW—gestational week. (G) RNA velocity is projected onto a predefined UMAP plot, hCOs (day 37) fixed and fresh cells combined. The length of the arrow annotates the transcriptional dynamics, and the direction of the arrow points to the future state of cells. Inset: potential indirect neurogenesis in hCOs. EBM, embryoid body medium; TPM, telencephalon patterning medium; NIM, neural induction medium; NM, neuronal medium; vRG, ventral radial glia; oRG, outer radial glia; IP, intermediate progenitors; EN, excitatory neurons; ventricular zone, VZ; subventricular zone, SVZ; intermediate zone, IZ; cortical plate, CP.

https://doi.org/10.1021/acschemneuro.3c00442
ACS Chem. Neurosci. 2023, 14, 3993−4012

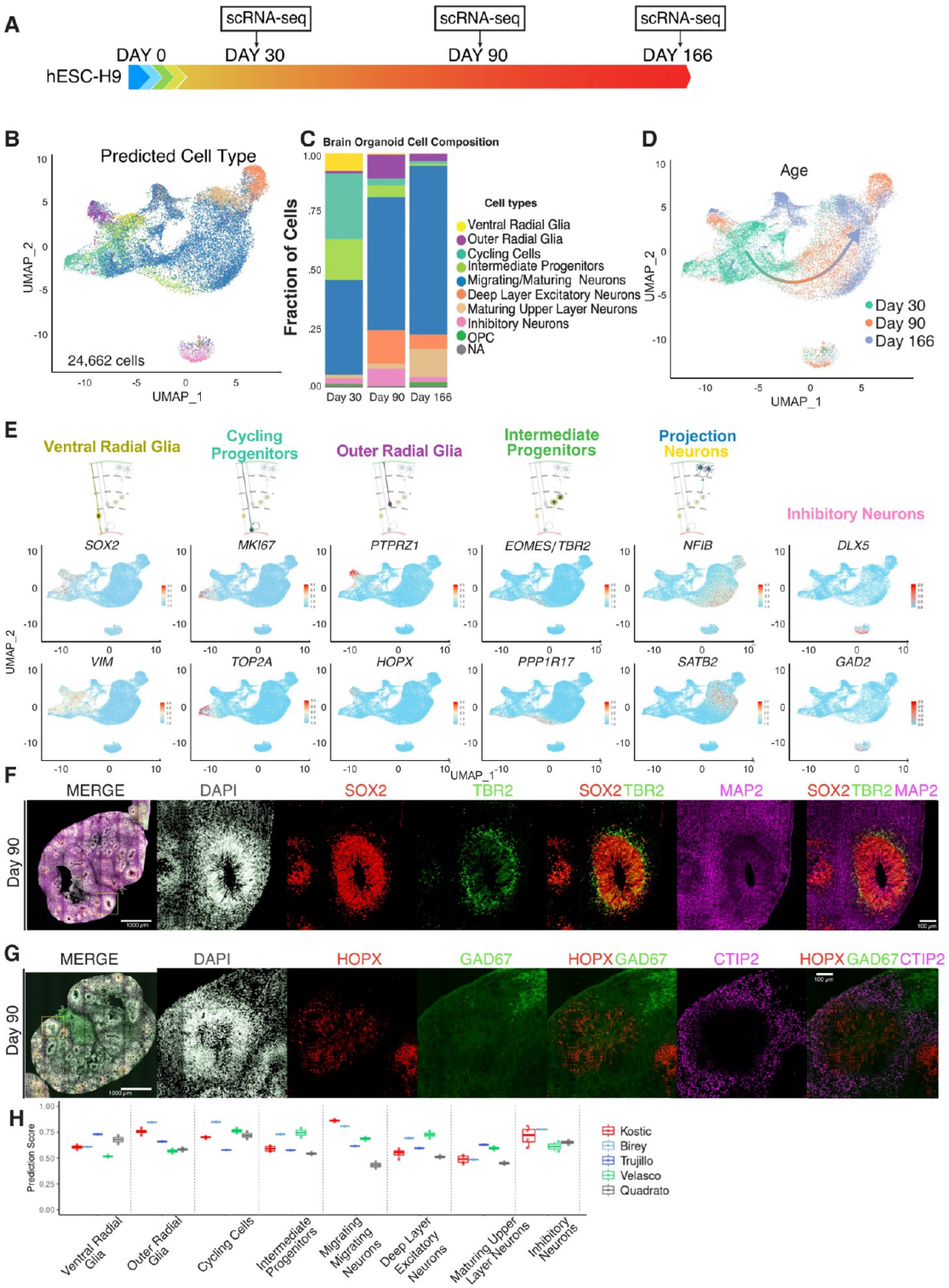

Figure 2. Longitudinal scRNA-seq profiling of hCO maturation. (A) Timeline of hCO differentiation, cell line hESC-H9. (B) scRNA-seq data set generated from three different ages of hCOs (day 30, day 90, and day 166; total = 24,662 cells), cell line hESC-H9. (C) Stacked bar plot showing relative distribution of cell types in hCOs measured by scRNA-seq split by age (day 30, day 90, and day 166), each column representing 10 randomly sampled organoids pooled and analyzed, cell line hESC-H9. (D) UMAP plot of hCO scRNA-seq data set split by age (day 30 [green] = 8955 cells, day 90 [orange] = 5969 cells, and day 166 [blue] = 10,011 UMAP plots showing expression of markers for main types of cells identified in hCOs, vRG (*SOX2* and *VIM*), cycling progenitors (*MKI67* and *TOP2A*), oRG (*PTPRZ1* and *HOPX*), IP (*EOMES* and *PPP1R17*), projection neurons (*NFIB* and *SATB2*), and INs (*DLX5* and *GAD2*). (F) Triple immunofluorescence for SOX2 (red), TBR2 (green), and MAP2 (magenta), combined with DAPI staining (white) of hCOs at day 90. Box indicates a representative neural rosette that is shown at a higher magnification; scale bars: 1000 and 100 μm, cell line hESC-H9. (G) Triple immunofluorescence for HOPX (red), GAD67 (green), and CTIP2 (magenta) combined with DAPI staining (white) of hCOs at day 90. Box indicates a representative neural rosette that is shown at a higher magnification; scale bars: 1000 and 100 μm, cell line hESC-H9. (H) Box plot showing prediction score for the identified cell type in scRNA-seq analysis of different data sets, split by protocol (guided and unguided protocols), (see Table S1).

https://doi.org/10.1021/acschemneuro.3c00442
ACS Chem. Neurosci. 2023, 14, 3993−4012

function.[19,20] In addition, hemiduplications, but not hemideletions, are associated with SCZ.[18,21]

Human brain development and behavior are different from that in rodents, and thus rodent models are insufficient to fully understand human disease.[22,23] The species divergence is particularly relevant for 16p11.2 CNVs because mice genetically modified for a chromosomal segment homologous to human 16p11.2 exhibit dissonant phenotypes relative to humans. For example, the hemideletion mice showed microcephaly and a low BMI, whereas the hemiduplication mice had a high BMI.[24,25] With the advent of the ability to reprogram human somatic cells into induced pluripotent stem cells (iPSCs),[26,27] we can now generate in vitro neuronal models for studying human disease mechanisms.[28−30] Previous studies have used two-dimensional (2D) iPSC neuronal models to examine the effects of 16p11.2 hemideletion and hemiduplication and identified the synapse, neurite, and dendrite length phenotypes, as well as transcriptional disruptions of genes outside of the 16p11.2 region.[31,32] Recently, three-dimensional (3D) human iPSC (hiPSC)-derived brain organoids have been used to improve the experimental modeling of brain development in physiological and diseased states.[33−37] With the advent of single-cell RNA sequencing (scRNA-seq),[38] it is now feasible to profile the transcriptional landscapes of brain organoids with cellular resolution.[37,39−42]

We aimed to better understand the disease mechanisms and affected cell types in 16p11.2 patients by leveraging human cortical organoid (hCO) models. To this end, we established a semiautomated protocol to generate and deeply characterize the cellular composition and cell-specific gene expression of hCOs by performing scRNA-seq at three differentiation time points. These data were integrated with a fetal brain atlas, and we observed that our hCO model recapitulated the crucial aspects of neurogenesis. We performed a large-scale guided differentiation of hCOs from 17 human iPSC lines derived from controls and patients with 16p11.2 hemideletion or hemiduplication. Using scRNA-seq as a readout, we observed reproducible cellular composition within and across the hCO lines. Importantly, we revealed the cell-type-specific changes in gene expression between hemideletion organoid models and controls. These differentially expressed (DE) genes are important for neurite formation, neuronal cell−cell adhesion, and synaptic processes and have been previously associated with neurodevelopmental disorders. Furthermore, the reduction in RBFOX1, an RNA-binding protein within ASD-associated CNVs, was validated at the protein level. Consistent with this, the RBFOX1 target mRNAs were disrupted in 16p11.2 patient organoids. Together, these data suggest that the cell-type-specific changes in gene expression may possibly contribute to developing a 16p11.2 pathogenic phenotype and that independent rare CNVs and resident genes may exhibit effects through convergent molecular signaling pathways.

RESULTS

Building a Platform for Robust hCO Generation. We modified the existing protocols using 3 patterning factors, with optimized doses and duration, to differentiate cells to neuronal lineages from human iPSCs into hCOs (see Methods section)[36,43] (Figure 1A). To scale up and minimize human error, we utilized an automated liquid-handling system (Hamilton STAR) during the most demanding part of the hCO differentiation protocol (until day 25) (Figure 1A) (see Methods section). Using single-cell transcriptomics, we aimed to compare a large-scale cohort of hCOs at different time points and batches. To reduce the technical challenges associated with working with the hCOs of many patients, we uncoupled the requirement of dissociating hCOs and performing scRNA-seq on the same day. Methanol fixation of the dissociated hCOs was optimized to enable long-term sample storage and the ability to rerun control samples during scRNA-seq library construction to control batch effects and monitor reproducibility[44] (Figure 1A).

First, the cellular diversity of hCOs was characterized under both fresh and fixed conditions by splitting a sample of 20 (10 fresh and 10 fixed) dissociated hCOs on day 37 of differentiation. Freshly dissociated and fixed cell suspensions were compared with scRNA-seq[45] (Figure 1A). In total, we profiled 9508 cells: 4939 fixed and 4570 fresh cells. We assessed cell quality, where cells with less than 5% of mitochondrial reads are judged to be of high quality.[46,47,96] The quality was similar for each condition, exhibiting less than 5% of reads aligning to mitochondrial transcripts (Figure S1A). We used Seurat's TransferAnchors function (see Methods section) to identify the putative cell types present in the hCOs (at day 37) by comparing them to fetal brain cells from a reference data set.[48] Both fresh and fixed hCO cells were compared to the reference data set of neocortical atlas.[48] When compared to the reference data set, both fresh and fixed hCOs contained all the main types of neuronal progenitors found in the fetal brain samples−ventral and outer radial glia (vRG and oRG; markers *SOX2* and *PAX6*), cycling cells (CycCells; markers *MKI67* and *TOP2A*), intermediate progenitors (IPs; markers *EOMES* and *HES6*), and different types of excitatory neurons including migrating/maturing neurons (MigNs/MatNs), expressing some level of *TBR1* and *NEUROD6* (Figure 1B,C,E).[47] Interestingly, we found a small population (<4% of total cell number) of inhibitory neurons (INs; markers *GAD2* and *DLX2*), similar to previous reports[37,41] (Figure 1B,C, and 1E). In addition, the majority of day 37 hCO cells were progenitor cell types with a small population of mature neurons (Figure 1F). Lastly, we found a minor population (<4% of total cells number) of oligodendrocyte precursor cells, microglia, pericytes, and endothelial cells. Overall, we found that methanol fixation does not significantly alter the transcriptional profile and cellular composition (Figures 1C,D, and S1B).

To analyze the lineage relationship between the predominant cell types, we performed RNA velocity analysis using velocyto.[49] The 10X Genomics scRNA-seq platform captures both unspliced and spliced mRNA. RNA velocity takes advantage of this by examining the relative abundance ratio of unspliced and spliced mRNA. This is used to estimate the transcriptional changes and the cell lineage direction. The most prominent lineage was originating from the neural progenitor cells, transiently crossing the IPs and differentiating into excitatory neurons (Figure 1G; red box). This suggests that the hCOs undergo indirect neurogenesis,[50−54] where the neural progenitor cells undergo asymmetric division to give rise to IPs, which eventually differentiate into excitatory cortical neurons. Together, these results show that the semiautomated platform for generating hCOs yields cells that model human embryonic neurogenesis.

Characterizing the Maturation of hCOs. To benchmark the cellular diversity of hCOs during maturation, we performed scRNA-seq on 30, 90 and 166 day old hCOs (Figure 2A−D). We methanol fixed the cells at each time point, which allowed

https://doi.org/10.1021/acschemneuro.3c00442
ACS Chem. Neurosci. 2023, 14, 3993−4012

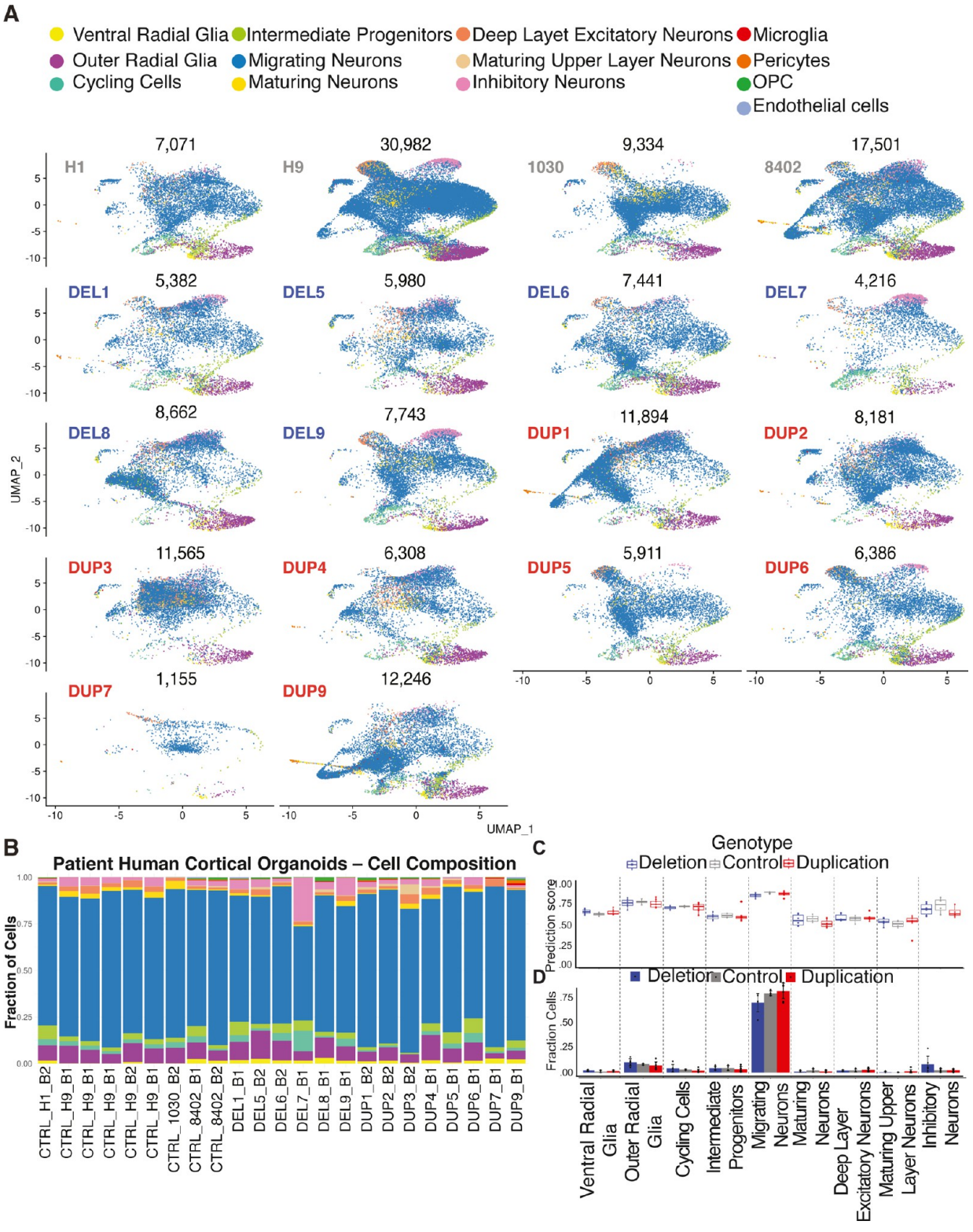

Figure 3. hCOs derived from control and 16p11.2 patient iPSC lines show similar cell composition. (A) scRNA-seq data UMAP embedding of individual iPSC lines from 90 day old hCOs after batch correction, control $n = 4$, hemideletions $n = 6$, and hemiduplication $n = 8$; total number of cells, 167,958. Note that CTRL_H9 and CTRL_8402 control lines contain higher numbers of cells as they were profiled throughout the multiple 10× single-cell runs (see also Figure S3D). (B) Stacked bar plots showing a relative distribution of cell types measured by scRNA-seq for 90 day old hCOs; each column represents an iPSC line, 10 randomly sampled organoids were pooled for each line. Note that CTRL_H9 and CTRL_8402 were profiled 5 and 2 times, respectively, in different experiments. (C) Box plot showing prediction score for the identified cell type in scRNA-seq analysis in hCOs, split by genotype, control $n = 4$, hemideletions (DEL) $n = 6$, and hemiduplications (DUP) $n = 8$. (D) Bar plot showing the average fraction of individual cell types per genotype in hCOs, control $n = 4$, hemideletions (DEL) $n = 6$, and hemiduplications (DUP) $n = 8$. Error bars represent the standard deviation.

https://doi.org/10.1021/acschemneuro.3c00442
ACS Chem. Neurosci. 2023, 14, 3993−4012

us to process all the samples for scRNA-seq at the same time to avoid batch effects. In total, we profiled 24,662 cells and identified 13 different cell types, of which 9 of the following cell types were predominant (~98.55% of total population): vRGs, oRGs, CycCells, IPs, MigNs, MatNs, deep-layer excitatory neurons (DlExNs), upper-layer neurons (UlNs), and INs (Figures 2B,C and S1C). At day 30, more than 50% of all cells were progenitors: vRG, oRG, CycCells, and IPs. By day 90, progenitor populations decreased to under 20%, and by day 166, vRG virtually disappeared. These changes were concomitant with a dramatic increase in neuronal populations (Figures 2B,C and S1C). Similar to previous experiments (Figure 1C), we detected INs expressing *DLX5* and *GAD2*, and the fraction of INs peaked at day 90 (Figure 2C,E). The fraction of oRGs (*PTPRZ1* and *HOPX*) increased from 1% (day 30) to 10% at day 90 and then decreased to 3% by day 166, which reflects human neurogenesis, where the peak of oRG production is in midgestational period of cortical development.[55−58] Additionally, 12% of cells at day 166 were identified as maturing upper layer excitatory neurons expressing (Figure 2C,E). This is consistent with temporal layer-specific patterning of neurons, with DlExNs being generated first in early neurogenesis and UlNs generation peaking in mid to late neurogenesis (Figure 2B−D).[59−61]

To gain insights into lineage dynamics, we performed RNA velocity analysis, where we combined cells from 3 developmental time points (day 30, day 90, and day 166) (Figure S1D−G). This analysis revealed a dynamic transition from neural progenitors to neurons. As observed in organoids from H1-hESCs (human embryonic stem cells) (Figure 1G), both 30 and 90 day old organoids from H9-hESCs also produced velocity vectors. H9-hESCs derived from 30 day old organoids showed evidence of a potential direct neurogenesis in which neuronal production stems from vRGs via transient progenitor population of IPs (Figure S1E). At day 90, H9-hESC-derived organoids also show signs of a potential indirect neurogenesis (Figure S1F), as seen in H1-hESCs (Figure 1G). Overall, we observed that the day 90 time point has sufficient representation of human brain-relevant cell types for subsequent disease modeling.

Next, we analyzed the cytoarchitecture of the hCOs. At day 90, we observed neural rosettes consisting of SOX2-positive neuronal progenitors tightly packed and radially aligned in a circular ventricular zone (VZ)-like structure (Figure 2F). Some of the SOX2-positive cells were positioned at the outskirts of the rosettes (Figure 2F). In addition, both rosettes and cell outskirt cells were also positive for the marker HOPX, together suggesting the presence of oRG-like cells (Figure 2F,G). Further, we detected a second concentric circle, the subventricular zone (SVZ)-like structure, composed of TBR2-positive IPs (marker *EOMES*), as found during fetal neurogenesis. We detected neuronal processes (marker MAP2-positive; Figure 2F) and deep-layer neurons (marker CTIP2-positive; Figure 2G). We also observed a portion of GAD67-positive INs, thus confirming the observation of INs by scRNA-seq (Figure 2G).

We compared our guided semiautomated protocol for generating hCOs to previously published protocols by comparing scRNA-seq data from our 90 day old hCOs to published data from brain organoids cultured for a similar length of time (Table S1).[36,37,40,41,62] Using Seurat's prediction score metric,[63] we were able to quantify each cell's similarity to each cell type from a reference fetal brain data set[48] (see Methods section). The type of each cell was predicted, and each cell was given a score between 0 and 1 based on how similar it was to that cell type (1 being the most similar). Prediction score analysis revealed that our hCOs were comparable to other guided brain organoid protocols (Figure 2H, Table S1).[36,37,41] However, the unguided (without addition of patterning factors) brain organoid protocol was the least similar to the human fetal brain, especially for excitatory neuronal cell types (Figure 2H). This analysis shows the semiautomated hCO protocol resulted in physiologically relevant cell types, similar to published guided brain organoid protocols[36,37,41] but with an increased throughput.

Large-Scale Differentiation of hCOs from Patient Lines Carrying 16p11.2 Hemideletion and Hemiduplication. The semiautomated production of hCOs recapitulates many aspects of human neurodevelopment, and 90 day old hCOs contain an optimal variety of cell types for modeling neurodevelopmental disorders. To test the ability of this platform for modeling human disease, we differentiated the hCOs from 17 different donor patient and control lines carrying a 16p11.2 pathogenic CNV (Figure S2). Out of 17 lines, 4 were controls, and the remaining 13 carried CNVs in 16p11.2 (6 hemideletion lines and 7 hemiduplication lines, of which 2 hemiduplications are clones). The hemideletion lines have similar CNVs (size 534 kb) encompassing 27 protein-coding genes, and the hemiduplication lines contain different CNV sizes (five 740, two 715, and one 534 kb), which encompass up to 30 protein-coding genes (Figure S2A). We confirmed the normal karyotype and presence of 16p11.2 CNVs using fluorescent in situ hybridization (FISH) and array comparative genomic hybridization (aCGH) for all the lines (Table S2; Figure S2B,C).

To profile the cell type diversity of the diseased hCOs, we performed scRNA-seq on 17 different healthy donor and patient cell lines at day 90 (Figures 3A and S3A−D). We split 17 lines into two differentiation batches. To determine the batch variability, two control lines, hESC-H9 (differentiation batch 1 and 2) and iPSC-8402 (differentiation batch 1 and 2), were included in both differentiations. In addition, to control for 10× library construction run, the hESC-H9-batch (B1) was included at each of 4 times performed (Figure S3B). Overall, we profiled 167,958 cells, of which the majority clustered in 9 main cell types (Figures 3A and S3C). First, we noticed that the hESC-H9 and iPSC-8402 control lines preserve the consistency of the cell types across the batches of differentiation and technical replicates of the same fixed sample for single-cell library construction (Figures 3B and S3D). Together, these data show that the semiautomated hCO protocol is highly scalable and reproducible. Next, we used cell prediction scores to assess the quality of the organoid cells in both patient and control samples. Prediction scores ranged from 0.6 to 0.8 across different cell types (Figure 3C). Importantly, we did not see a significant difference in cell type prediction scores across genotypes (control, hemideletion, and hemiduplication; Figure 3C). This indicates a similar cell type fidelity to fetal brain tissue across genotypes.

To determine whether the presence of the 16p11.2 CNV alters cell composition during development, we quantified the percentage of each cell type across the patient organoids. We did not detect significant differences in cell type composition between the genotypes (Figure 3D). We observed non-significant trends of MigNs decreasing in deletions and INs increasing in deletions (Figure 3D). Similar fractions of cell

https://doi.org/10.1021/acschemneuro.3c00442
ACS Chem. Neurosci. 2023, 14, 3993−4012

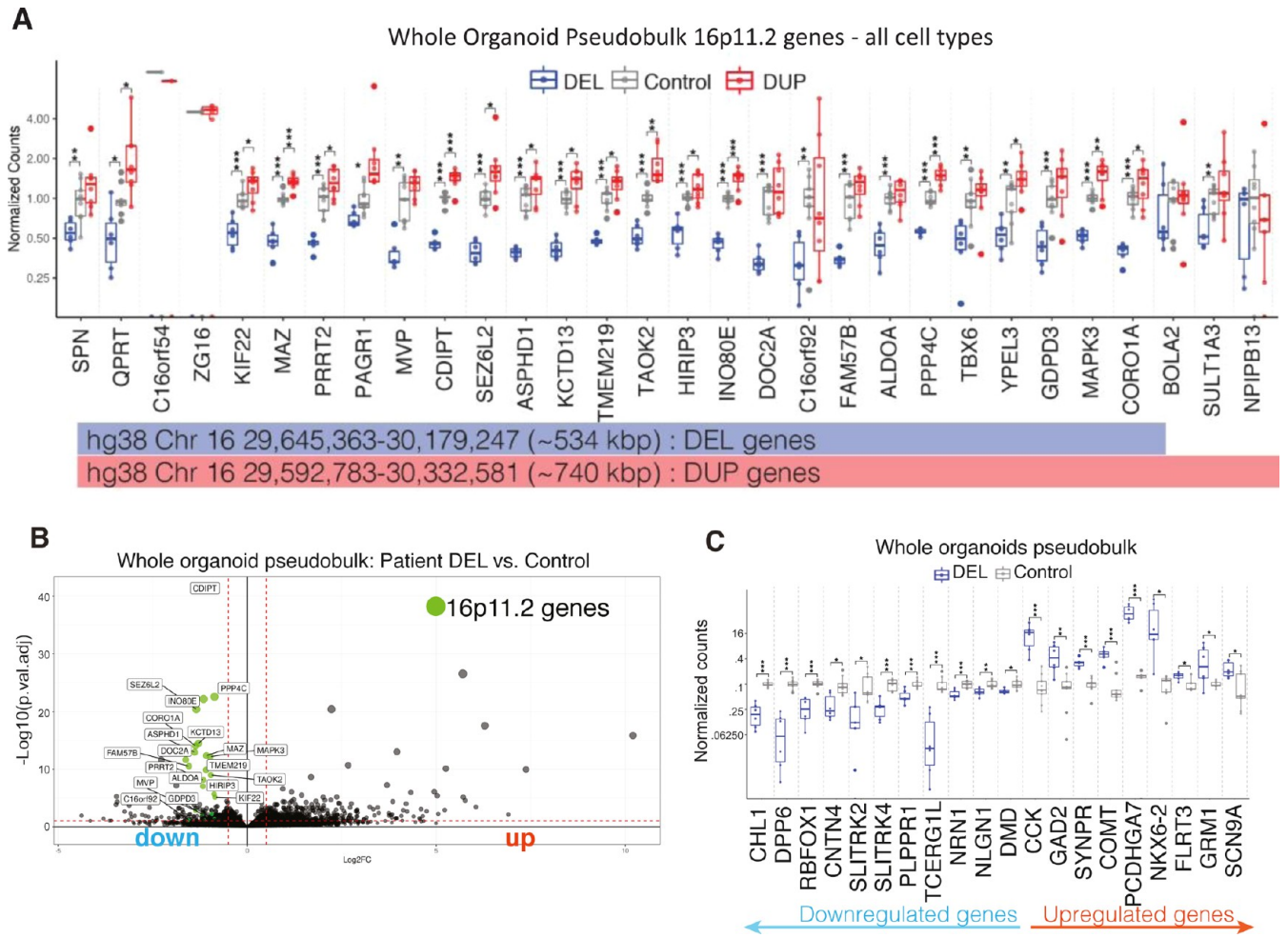

Figure 4. 16p11.2 hemideletion alters gene expression within and outside of locus in patient-derived cortical organoids. (A) Expression of 16p11.2 genes in hCOs (day 90), pseudobulk analyses in deletion (DEL, blue), control (gray), and duplication (DUP, red); blue and red lanes below the graph represent the most common CNV (hemideletion [534 kbp] or hemiduplication [740 kbp]) of the donors analyzed. Each dot presents a cell line. The *Y*-axis represents normalized counts $*p < 0.05$, $**p < 0.01$, $***p < 0.001$ (ANOVA test). (B) Volcano plot showing DE genes in patient hemideletions vs control lines, all cell types collectively; 16p11.2 genes are colored green; cutoff-adjusted *p*-value <0.1. (C) Selected DEGs that are downregulated and upregulated in patient hemideletion (DEL) vs control hCOs. $*p < 0.05$, $**p < 0.01$, $***p < 0.001$ (ANOVA test).

types across different donor lines indicate the reproducibility of the hCOs (Figure 3C,D). While we detected some differences between individual donors, when the data was analyzed by genotype, we did not observe a significant alteration in the differentiation propensity for either 16p11.2 hemideletion or hemiduplication lines.

Cell-Type-Specific Alteration of Gene Expression by 16p11.2 Hemideletion. First, to confirm the primary effect of the 16p11.2 CNV, we looked at the normalized expression of 16p11.2 gene counts across each genotype. We found significant downregulation of genes in hemideletion donors within the 16p11.2 region (Figure 4A). In contrast, only a few 16p11.2 genes were DE in hemiduplication donor lines (Figure 4A). Next, we aggregated data from all single cells in each organoid into a pseudobulk transcriptome and performed differential expression across genotypes. From this analysis, we detected ∼50% downregulation of 24/27 genes in 16p11.2 deletion lines (volcano plot genotype averaged, Figure 4B) (see Methodssection). In addition, we detected multiple DE genes outside of the 16p11.2 locus (Figure 4C). However, hemiduplications show only a few significantly upregulated, DE 16p11.2 genes (volcano plot, Figure S4A). This is consistent with the lower penetrance of 16p11.2 hemiduplication relative to hemideletion.[64] After examining the expression of the 16p11.2 genes, we concluded that the hemideletion samples have a stronger primary deficit and exhibited reduced expression for a higher percentage of the 16p11.2 resident genes in the whole organoid pseudobulk sample compared to the hemiduplication lines. At day 90, hemideletions also perturb more genes outside of the 16p11.2 locus, indicating a stronger phenotype at this developmental stage. In other studies, the hemideletion consistently produced larger gene expression changes in expression in human lymphoblastoid cells, more severe behavioral phenotypes in mice, and a higher penetrance of phenotypes in humans.[64−67]

Next, we examined the differential expression across cell types separately for hemideletion and hemiduplication. In hemideletion hCOs, the downregulated genes were mostly observed in migrating neurons, while the upregulated genes were mostly observed in radial glia and migrating neurons (Figures 5 and S5A,B). In hemideletions, we identified 114 DE genes, with 38 downregulated and 76 upregulated across nine cell types (Figure 5, Table S3). Consistent with the relatively low effect on 16p11.2 gene expression, hemiduplication had 70

https://doi.org/10.1021/acschemneuro.3c00442
ACS Chem. Neurosci. 2023, 14, 3993−4012

A

Genotype		Total / cis / trans genes	vRG	oRG	CycCell	IP	MigN	MatN	DL_ExN	Mat_UL_N	IN
DEL	↓	38 / 17 / 21	2	13	7	7	24	12	13	2	8
	↑	85 / N.A. / 85	2	32	8	4	33	20	12	1	8
DUP	↓	10 / N.A. / 10	–	–	–	1	1	8	–	2	–
	↑	60 / 3 / 57	3	10	3	6	19	43	3	1	1

B

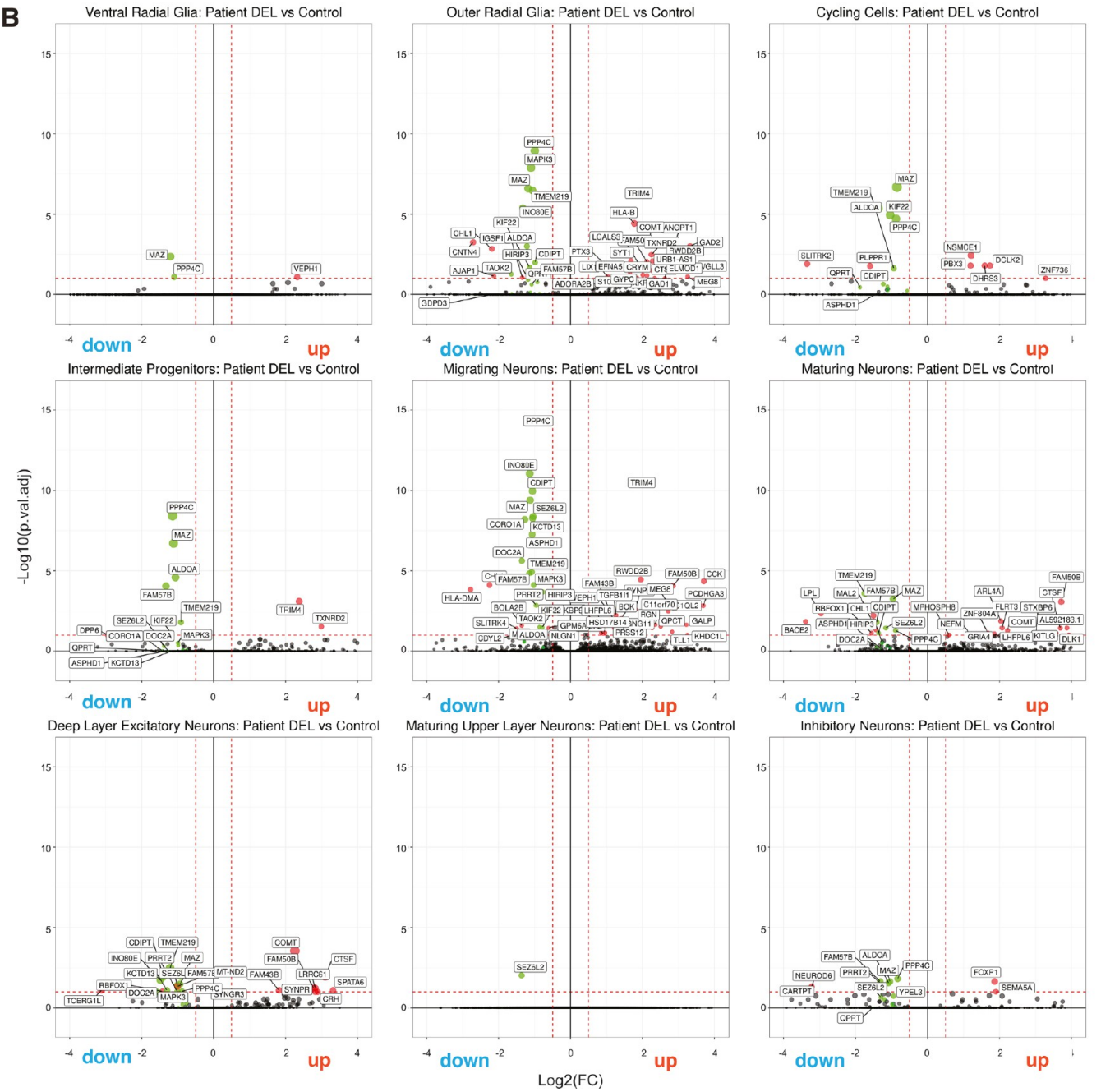

Figure 5. Hemideletion of 16p11.2 patient hCOs exhibiting cell-type-specific alterations of gene expression. (A) Table showing number of genes that are downregulated and upregulated in patient hemideletions vs control (blue rows), and patient hemiduplication vs control (red rows), split by the cell type (columns). Cis = genes within 16p locus. Trans = genes outside of the 16p locus. (B) Volcano plots showing DE genes in patient hemideletions (DEL) vs control lines, split by the cell types; 16p11.2 genes are colored green, and selected DEGs are colored red; cutoff-adjusted *p*-value <0.1. vRG, ventral radial glia; oRG, outer radial glia; CycCell, cycling cells; IP, intermediate progenitors; MigN, migrating neurons; MatN, maturing neurons; Dl_ExN, deep-layer excitatory neurons; May_Ul_N, maturing upper-layer neurons; IN, inhibitory neurons.

DE genes, of which 10 were downregulated and 60 were upregulated (Figure 5A). Hemideletion DE genes had overlapping genes across the individual cell types, whereas hemiduplication lines exhibited fewer overlapping DE genes (Figure 5, Table S3). Notably, in hemideletion hCOs, *DPP6*, *RBFOX1*, and *TCERG1L* were each downregulated in several

https://doi.org/10.1021/acschemneuro.3c00442
ACS Chem. Neurosci. 2023, 14, 3993−4012

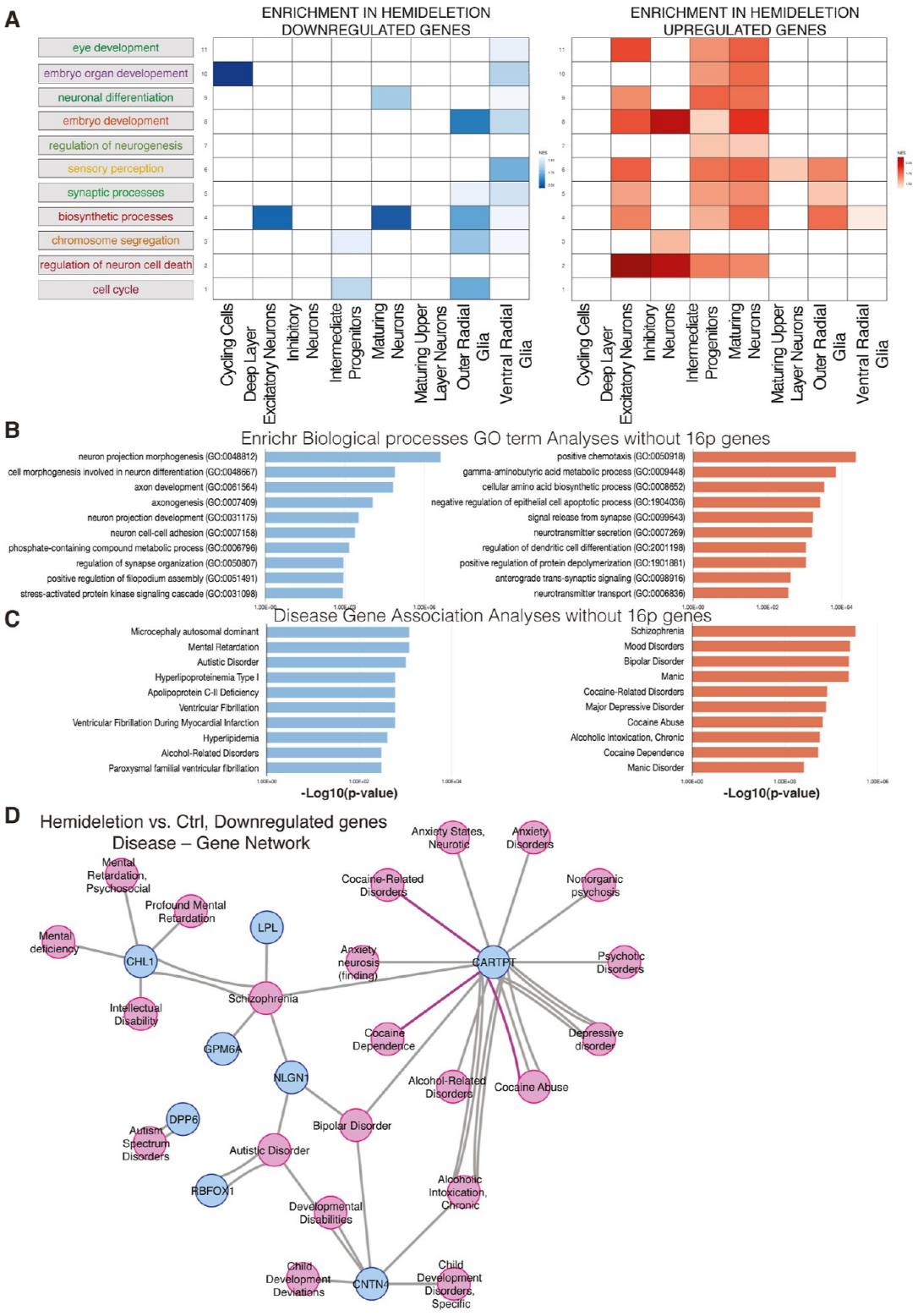

Figure 6. Functional categories, GO, and disease−gene enrichment analysis of 90 day old cortical organoids in control and 16p11.2 patient hemideletion lines. (A) Enrichment of functional categories derived from GO clustering of genes that are downregulated and upregulated in hemideletions, split by cell types (NES, normalized enrichment score); (see Table S4). (B) Top 10 GO: biological processes for downregulated (blue) and upregulated (red) genes in hemideletions (cutoff-adjusted p-value < 0.1), ordered by their enrichment p-value; the x-axis is converted−log 10(p-value) (see Table S4). (C) Top 10 gene−disease associations for downregulated (blue) and upregulated (red) genes in hemideletions (cutoff-adjusted p-value <0.1), ordered by their enrichment p-value; the x-axis is converted−log 10(p-value) (see Table S5). (D) Graphical representation of the gene−disease network for downregulated genes in patient hemideletion hCOs (see Table S5).

cell types and are previously associated with ASD and attention-deficit hyperactive disorder (Figure 5).[68−70] Furthermore, we found the downregulated genes grouped across cell types that play a role in neuronal cell adhesion, which were

https://doi.org/10.1021/acschemneuro.3c00442
ACS Chem. Neurosci. 2023, 14, 3993−4012

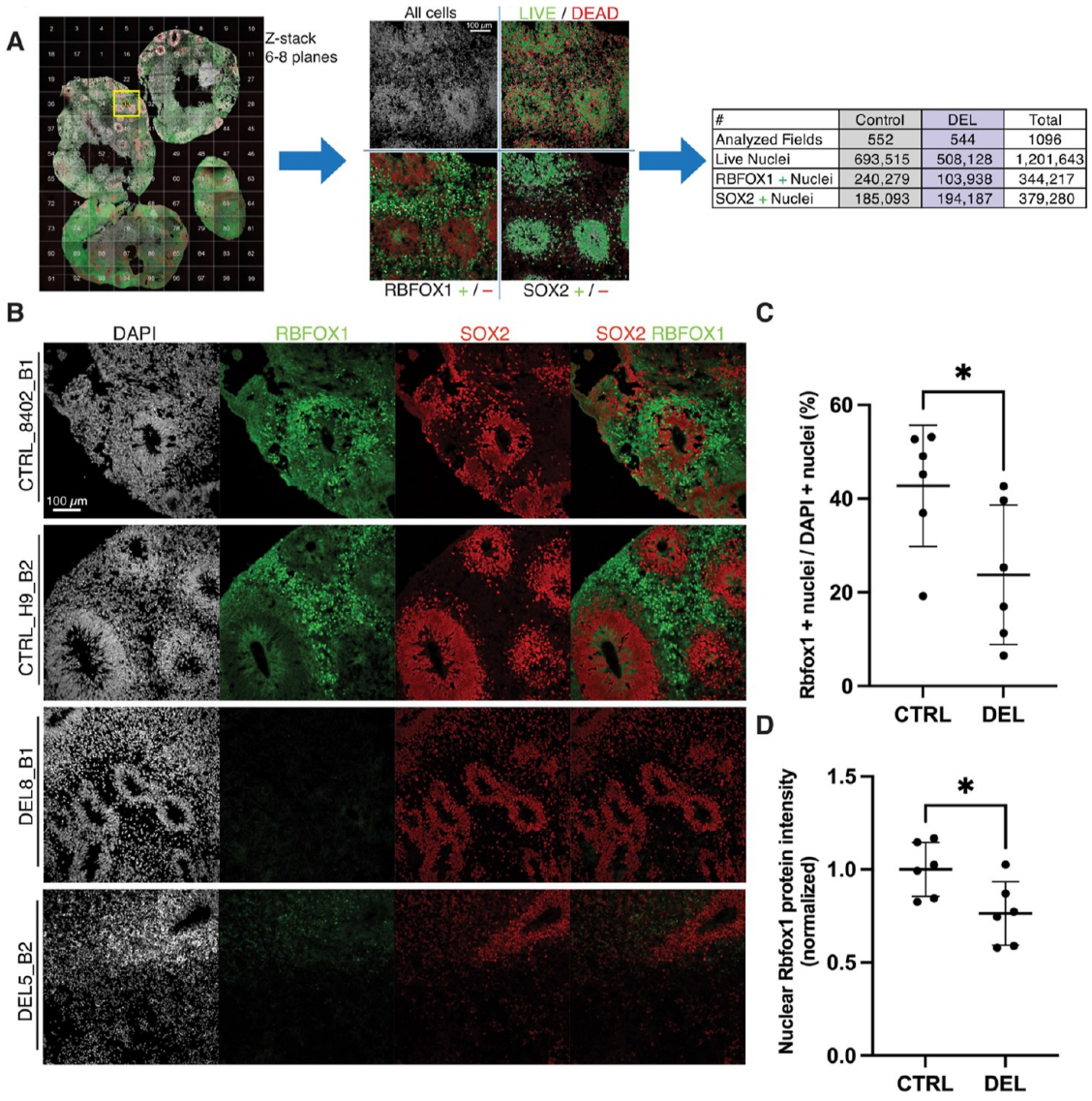

Figure 7. 16p11.2 hemideletion of hCOs exhibits reduced expression of RBFOX1. (A) High-content imaging of hCO cryosections and strategy to detect live cells, RBFOX1-positive cells, and SOX2-positive cells. (B) Double immunofluorescence for RBFOX1 (green) and SOX2 (red), combined with DAPI staining (white), of hCOs at day 90; selected cell lines CTRL_8402_B1, CTRL_H9_B2, DEL8_B1, and DEL5_B2; scale bars: 100 μm. (C) Quantification of the percentage of RBFOX1-positive nuclei over total number of nuclei determined by DAPI on cryosections (20 μm) in control (CTRL, n = 6) and hemideletion (DEL, n = 6) 90 day old hCOs. Each data point presents an independent cell line, with CTRL_H9 and CTRL_8402 differentiated in two different batches. The mean ± SD is shown; *p < 0.05 (t-test) (see Table S6). (D) Quantification of the nuclear intensity of the RBFOX1 fluorescent signal in all live cells (determined by DAPI, see Methodssection) on cryosections (20 μm) in control (CTRL, n = 6) and hemideletions (DEL, n = 6) 90 day old hCOs. Average intensity of the fluorescent signal value of all controls was used to normalize data. Each data point presents an independent cell line, with CTRL_H9 and CTRL_8402 differentiated in two different batches. The mean ± SD is shown; *p < 0.05 (t-test), (see Table S6).

previously associated with ASD including *CHL1*, *CNTN4*, and *NLGN1*[71−74] (Figure 5). Interestingly, independent studies showed pathogenic CNVs within *RBFOX1*, *DPP6*, *CNTN4*, *NLGN1*, and *CHL1* in patients suffering from several different neurodevelopmental disorders.[5,75−77] Additionally, *COMT* was upregulated in 3 of 9 identified cell types. *COMT is* located in the pathogenic CNV 22q11.2 and was identified as a risk gene for SCZ.[78] Therefore, our analysis of 16p11.2 hemideletion hCOs has identified a potential convergence of the 16p11.2 deletion syndrome with other genes previously implicated in neurodevelopmental disorders.

Pathway and Gene−Disease Network Analysis in Hemideletion Patient Lines. Because hemideletion lines exhibit a stronger transcriptional phenotype in our hCO model, we focused our secondary analysis on the DE genes. To investigate which processes are enriched across cell type populations, we performed pathway analysis. First, using gene set enrichment analyses (GSEAs), we identified 11 different clusters containing gene ontology (GO) and biological processes (BP) IDs (Figures 6A and S6A, Table S4). Next, we designated relevant functional categories for each of these 11 clusters based on the most common GO IDs (Figure S6A) (see Methods). The most robust enrichment of different functional categories was observed in oRGs, vRGs, IPs, MatNs, and DlExNs (Figure 6A). We detected prominent enrichment of the upregulated genes in several neuronal populations in multiple clusters (e.g., response to neuron cell death, biosynthetic processes, synaptic processes, sensory perception,

https://doi.org/10.1021/acschemneuro.3c00442
ACS Chem. Neurosci. 2023, 14, 3993−4012

regulation of neurogenesis, and neuronal differentiation). This suggests a change in the maturation of the excitatory neurons in hemideletion patient lines, similar to the observations made using a 2D directed differentiation of hemideletion patients' iPSCs to neurons.[31] In addition, highly proliferative oRGs and IPs were enriched in cell cycle, chromosome segregation, and biosynthetic processes (clusters 1, 3, and 4). Lastly, multiple DE genes in hemideletions were brain-specific genes (Figure S6B,C).

To specifically elucidate the pathways associated with DE genes outside of the 16p11.2 locus, we excluded 16p11.2 genes and performed GO: BP term analysis of downregulated and upregulated genes in hemideletions, using the Enrichr gene analysis platform.[79−81] The downregulated genes were implicated in neuron projection morphogenesis, neuron cell−cell adhesion, axon development, and other terms implicating neurite process assembly and neuron-to-neuron interaction (Figure 6B). This result is consistent with a recent study, which identified defects in neuronal migration in 16p11.2 hemideletion hCOs.[82] Furthermore, the upregulated genes were implicated in synaptic-relevant processes, such as signal transmission and neurotransmitter biosynthesis and transport (Figure 6B, Table S4). Together, gene enrichment analysis shows signatures of disrupted neuronal maturation and synaptic function in 16p11.2 hemideletion hCOs.

To investigate a direct link between DE and disease genes, we used the Cytoscape disease−gene network tool to perform disease gene enrichment (Figure 6C, Table S5).[83,84] We found that microcephaly, ID, and autistic disorder were the top three enrichments for downregulated genes. Moreover, we generated a disease−gene network for downregulated genes, which illustrates that several genes (*RBFOX1*, *CNTN4*, *DPP6*, *CHL1*, and *NLGN1*) converge upon neurodevelopmental and neuropsychiatric disease−gene networks (Figure 6C,D). In addition, analysis of the upregulated genes identified enrichments in SCZ, mood disorders, and bipolar disorder. Together, disease−gene enrichment analysis suggests that in hemideletion hCOs, the DE genes located outside of the 16p11.2 region are associated with neurodevelopmental disorders.

16p11.2 Patient hCOs Exhibit Reduced RBFOX1 Protein Expression. *RBFOX1* is a critical neuron-specific regulator of alternative splicing in human neurodevelopment.[2] Similar to 16p11.2 deletions, haploinsufficiency of the region in 16p13.3 containing *RBFOX1* is associated with ASD, epilepsy, and ID.[1] We found that *RBFOX1* mRNA is downregulated in 16p11.2 hemideletion patient hCOs, specifically within the neuronal cell types (Figures 5B and S7A,B). We reasoned that a lower mRNA expression of *RBFOX1* in hemideletion patient lines would result in lower protein expression. To check this, we used SOX2 and RBFOX1 antibodies to perform immunohistochemistry on fixed 20 μm thick hCO cross sections. As expected, SOX2 and RBFOX1 showed nuclear localization in mutually exclusive cell populations (Figure 7A). SOX2-positive nuclei, as seen before (Figure 2F), were labeling neural progenitor rosettes, while RBFOX1-positive nuclei were found in adjacent neuronal populations (Figure 7B). To quantify the intensity of nuclear RBFOX1 and SOX2 fluorescence, we used a high-content imager. On average, we analyzed 3 fluorescently labeled cross sections from 3 independent 90 day old hCOs per cell line (6 control lines [CTRL_H9 batch 1 and 2; CTRL_8402 batch 1 and 2; CTRL_H1; and CTRL_1030] and 6 lines from individual hemideletion patients). Prior to quantification, we trained the software to do the following steps: (1) recognize all nuclei using 4',6-diamidino-2-phenylindole (DAPI) staining; (2) distinguish live and dead (pyknotic) nuclei based on nuclear size and fluorescent brightness intensity; (3) identify RBFOX1-positive nuclei; and (4) identify SOX2-positive nuclei (Figure 7A). Overall, we measured the intensity on 1096 different fields, containing 1,201,643 live cells, out of which 344,217 nuclei were positive for RBFOX1 (Figure 7A, Table S6). We found that the percentage of RBFOX1-nuclear positive cells was significantly lower in the hemideletion lines (Figure 7C). In addition, the RBFOX1 nuclear intensity was significantly decreased in hemideletion lines (Figure 7D). In contrast, the percent of SOX2-positive nuclei and SOX2 nuclear intensity was comparable between the controls and hemideletions (Figure S7C,D). This confirms our earlier observation by scRNA-seq that neural progenitor number is comparable in patient-derived hemideletions and controls, concurring with Deshpande et al. 2017.[31] We noted variability in the nuclear RBFOX1 intensity, which could be due to different patient donors. This is not surprising, given the incomplete penetrance and genetic heterogeneity of neurodevelopmental disorders.[6,64,85]

After confirming the reduction of RBFOX1 protein in 16p11.2 hemideletion hCOs, we next looked for evidence that a reduction in RBFOX1 could influence the changes in gene expression observed in 16p11.2 hCOs. RBFOX1-dependent splicing events and secondary changes in gene expression have been previously determined by performing RNA-seq after *RBFOX1* knockdown in differentiated primary human neuronal progenitors.[2] In that study, RBFOX1 regulated 1560 genes, which were enriched for regulators of neurodevelopment and autism. By comparing these published RBFOX1 targets to the DE genes we identified in the 16p11.2 hemideletion hCOs by pseudobulk RNA-seq analysis, we found that ∼21% of the DE genes were also regulated by RBFOX1 (24 of 114 genes, adjusted-p < 0.1, whole data set, pseudobulk; Figure 4B,C, Table S7). Some of the 24 genes that overlap between 16p11.2 hCOs and RBFOX1 targets have been previously linked to neurodevelopmental disorders (e.g., *NLGN1*, *CHL1*, *SLITRK2*, *SYNPR*, *CRH*, *DCLK2*, *TCF7L2*, *GAD1*, *GAD2*, and *LGALS3*).[76,86−88] Overall, these data suggest that the reduction in RBFOX1 protein in 16p11.2 hemideletion hCOs may possibly be responsible for some of the differential gene expression and indicate the existence of a common molecular signature across independently associated neurodevelopmental risk loci.

DISCUSSION

This study generated single-cell transcriptional profiles from 16p11.2 heterodeletion patients and controls in a complex 3D human organoid model, which recapitulates early human brain development in vitro. We found that hCOs have transcriptional similarities with the developing fetal neocortex atlas.[48] The hCOs showed a clear maturation trajectory along the neuronal lineage from neural progenitor cells to mature neurons at the oldest profiled age (166 days). In addition, our analysis of lineage relationships suggested an occurrence of crucial events such as direct and indirect neurogenesis.[50−54] By using automation, we were able to standardize and scale up production to generate hundreds of hCOs to model neurodevelopmental disease using 17 patient and control cell lines. By performing scRNA-seq on over 150,000 cells, we

https://doi.org/10.1021/acschemneuro.3c00442
ACS Chem. Neurosci. 2023, 14, 3993−4012

demonstrated similar cellular composition across cell lines and batches of independent differentiations. The robust large-scale patterned organoid differentiation presented here leveraged automation to produce cells similar to the fetal brain at a sufficient scale to identify a transcriptional signature in 16p11.2 hemideletion. Furthermore, we were able to utilize high-throughput quantification of immunofluorescence-stained organoid sections to validate the reduction of RBFOX1 at the protein level by examining more than a million cells across patients and controls. Overall, this demonstrates that brain organoids at scale will continue to play a critical role in neurodevelopmental disease modeling. In the future, organoids will become increasingly important for drug discovery projects aimed at demonstrating the efficacy, specificity, and safety of new treatments in patient cell lines.

By modeling 16p11.2 CNVs with patient-derived hCOs in combination with scRNA-seq, we elucidated the changes in the expression of genes previously implicated in neurodevelopmental disorders. Most of the transcriptional changes we found in the hemideletion lines were specific to neuronal cell types, and gene enrichment analysis showed neuronal maturation- and synaptic function-relevant signatures in hemideletion patients. Despite the apparent methodological differences, the overall finding of increased neuronal maturation in hemideletions was similar to a recent study using 3D brain organoids.[82] We observed minimal changes in the hemiduplication lines. There were fewer DE genes and less overlap across cell types. More work will be needed to identify relevant phenotypes in duplication lines, and this may require a broader range of developmental time periods and the use of additional phenotypic assays.

Here, we identified a shared molecular signature between independent neurodevelopmental risk loci, the 16p11.2 CNV and the *RBFOX1* gene, both of which present a similar spectrum of clinical phenotypes in ASD, ID, SCZ, and epilepsy.[1,3,5] Previous studies indicate three 16p11.2 genes (*KCTD13*, *HIRIP3*, and *ALDOA*), which were found to be RBFOX1-dependent genes, suggesting a reciprocal interaction between the 16p11.2 and RBFOX1 CNV loci. Consistent with this, studies in *Drosophila melanogaster* identified evidence for interactions between 16p11.2 homologue genes and neurodevelopmental genes. Loviglio and colleagues[15] indicated that the 16p11.2 region is a chromatin hub for ASD and detected the chromatin contacts between the 16p11.2 region and additional ASD genes such as *PTEN*, *TSC2*, and *CHD1L*.[15,89−91] Weiner and colleagues have identified that both rare and common genetic risk for ASD are present and interact on chromosome 16p.[92] For future studies, it will be interesting to determine the molecular determinants of this potential network of 16p11.2-regulated gene expression.

Modeling of 16p11.2 using 2D/3D iPSC brain models has been conducted by several laboratories.[32,65,82,93] Urresti et al., and Sundberg et al. have identified consistent alterations in RHOA.[65,82] Tai et al., identified changes in GABAergic neurons and the balance between inhibitory and excitatory neuronal activity.[93] Roth et al., identified gene expression changes in neuronal progenitor stages.[32] There are several potential sources for variation between studies, including different patient lines, differentiation protocols, and different assays. This study here, linking the 16p11.2 CNV with *RBFOX1* mRNA regulation on the same chromosome arm (16p13.3), is conceptually most like that by Weiner et al. 2022, where the authors identified that common polygenic risk and the rare 16p11.2 CNV regulate ASD genes on the same chromosomal arm. Future studies will be needed to identify the consistent signals present among patients. This confirmation will then enable identification of novel drug targets or biomarkers in pursuit of drug development for ASD. To work toward this goal, it will be critical for cross-laboratory collaboration using carefully selected patient cohorts of large sample sizes to identify translatable in vitro phenotypes.

In this study, many genes disrupted in 16p11.2 hCOs have also been independently connected to neurodevelopmental disease. Like *RBFOX1*, we also identified differential expression of other notable CNV genes such as *DPP6*, *NLGN1*, *CHL1*, and *CNTN4*, which are also associated with neurodevelopmental and neuropsychiatric disorders.[5,75−77] Future studies will be required to determine how broadly this spectrum of genetic variants may interconnect phenotypically similar but genetically distinct clinical cases. Regardless of the outcome, this may inform therapeutic discovery strategies in terms of whether to focus on the common pathways to treat a spectrum of disorders or personalized therapeutics to treat narrow and defined groups of patients. Our work here provides evidence of the former and encourages the rational synergy of therapeutic discovery between mechanistically overlapping neurodevelopmental disorders.

METHODS

hPSC Lines. A total of 18 hPSC lines were used in this study. Four control lines, out of which 2 are hESC and 2 hiPSC. Patient-derived iPSCs lines that carry 16p11.2 CNV were split into hemideletions (6) and hemiduplication (8). Each hPSC line represents the individual donor, except two clone lines, DUP3 and DUP7, which are derived from the same patient. Detailed description of the cell lines is provided in Table S2. Material transfer agreements were arranged with Stanford, NIH, and Simons foundation to procure iPSC lines from consenting patients in this study.

CNV Analyses and Karyotyping. To verify CNVs (hemiduplication and hemideletion) in 16P11.2 patient iPSC lines, the aCGH tests were performed. FISH was performed to evaluate the purity of patient lines. The FISH probes were designed to detect signals within chr16:29729098−29909316 in hg38 (UCSC Genome Browser). All lines used in this study were karyotypically normal. aCGH and FISH tests were performed by Cell Line Genetic (Table S2). Karyotyping was performed by Cell Line Genetic or WiCell. See Table S2 for results of the karyotyping, aCGH, and FISH analysis.

Culture of hPSCs. Feeder-free hPSCs were cultured on the 6-well plates (VWR, 10861−554) that were coated with Matrigel (Corning, 354277, lot no. 9203011) in mTeSR Plus (StemCell Technologies, 05825). Cells were passaged when confluence of 70−80% was reached using ReLeSR (StemCell Technologies, 05872) to detach and dissociate the colonies, which were then transferred to the mTeSR Plus with 0.2 μM thiazovivin added (EZSolution, 1736). All cell lines were karyotypically normal, and testing was performed by WiCell and Cell Line Genetics. The hPSC lines were tested negative for mycoplasma.

Cortical Organoid Differentiation Protocol. hPSCs were grown in mTeSR Plus. On day 0, the cells were inspected under a bright-field microscope to check for differentiation. Cells were used for cortical organoid differentiations when they reached 70−80% of confluence. Prior to lifting the cells, undifferentiated hPCS were primed for 2 h with 50 μM Y-27632 ROCK inhibitor at 37 °C (Selleckchem, S1049), diluted in mTeSR Plus. Cells were incubated 6−7 min in Accutase (Gibco, A1110501) at 37 °C. To obtain a single-cell suspension, 4−5 trituration cycles were performed with a P1000 pipet. mTeSR Plus with 50 μM Y-27632 was added to neutralize Accutase, and the cells were transferred to 15 mL tube, spun down 5 min at 200*g*, resuspended in 5 mL of mTeSR Plus with 50 μM Y-27632 and strained through 40 μM strainer (Grainer,

https://doi.org/10.1021/acschemneuro.3c00442
ACS Chem. Neurosci. 2023, 14, 3993−4012

542040). hPSCs' viability and counts were determined on a Vi-CELL XR cell viability analyzer (Beckman Coulter, 731050). To continue the differentiation protocol, the viability had to be above 80%. The cells were diluted in mTeSR Plus with 50 μM Y-27632 to 60,000 cells/ml, and 150 μL of cells or ∼9000 cells/well was transferred to ultralow attachment (ULA) 96-well plates (Greiner, 650979). Lastly, the cells were spun for 1 min at 150*g*. On day 2, hPSC embryoid bodies were inspected under the bright-field microscope. 120 μL of mTeSR Plus with 50 μM Y-27632 medium was replaced with 130 μL of only mTeSR Plus medium. From this step on, all the feedings of embryoid bodies/cerebral organoids in ULA plates were performed on an automated liquid-handling robot system (Microlab STAR Liquid Handling System, Hamilton Co.). Each cycle of automated feeding performs the following steps: (1) aspirate−dispense 100 μL to lift the dead cell debris, (2) wait 15 s for cortical organoid to settle, (3) aspirate 100 μL of old medium, and (4) add 100 μL of fresh medium. From day 3 to day 7, the cerebral organoids were fed with telencephalon patterning medium (TPM): DMEM/F12, GlutaMAX (Gibco, 10565018), 1× KnockOut Serum Replacement (Gibco, 10828010), 1× penicillin−streptomycin (Gibco, 10378016), 2× GlutaMAX (Gibco, 35050061), 1× MEM non-essential amino acids solution (Gibco, 11140050), 1× 2-mercaptoethanol (Gibco, 21985023), 5 μM dorsomorphin (StemCell Technologies, 72102), 10 μM SB431542 (StemCell Technologies, 72234), and 2 μM XAV939 (StemCell Technologies, 72674). TPM was changed every day from day 3 to day 7. From day 8 to day 25, the medium was changed to neural induction medium (NIM): DMEM/F12, GlutaMAX, and Neurobasal (Gibco, 21103049) in vol/vol 1:1 ratio, 1× B-27 minus vitamin A (Gibco, 12587010), 1× N-2 supplement (Gibco, 17502048), 0.75× GlutaMAX, 1× penicillin−streptomycin−glutamine, MEM non-essential amino acids solution, 1 μg/mL heparin (Millipore Sigma, H4784), 20 ng/mL EGF (R&D systems, 236-EG-01M), and 20 ng/mL FGF (R&D systems, 233-FB-025) both reconstituted in 0.1% bovine serum albumin. From day 16 to day 25, B-27 without vitamin A is replaced with 1× B-27 with vitamin A (Gibco, A3582801). On day 26, the organoids were transferred to 100 mm petri dishes (Corning, CLS3262). From day 26 to 42, the medium was changed to neuronal medium that has same base recipe like NIM, but instead of EGF and FGF, it contains 20 ng/mL BDNF (Peprotech, 450−02) and 20 ng/mL NT3 (Peprotech, 450−03), both reconstituted in 0.1% bovine serum albumin. After day 43, the organoids were weaned from BDNF and NT3.

Cortical Organoid Dissociation and Methanol Fixation. Cortical organoid dissociation was performed using the Neural Tissue Dissociation Kit, enzyme (P), (MACS Mitenyi Biotec, 130−092−628). In brief, organoids, 10−30 depending on the size and age, were pooled together, and dissociation was performed following the manufacturer's protocol, program 37C_NTDK_1, using gentleMACS OctoDissociator with heaters (MACS Mitenyi Biotec, 130−096−427). Upon dissociation, the cells were strained through a 40 μM strainer to achieve single-cell suspension. The cells were spun down for 10 min at 300*g*, the supernatant was discarded, and the cells were resuspended in 1 mL ice-cold 1× PBS. Cell number and viability were determined with acridine orange (AO)/ propidium iodide (PI) staining on an automated cell counter (Nexcelom, Cellometer Auto 2000). To fix the cells, 9 mL of ice-cold 100% methanol was added to the cell suspension in a dropwise manner to prevent cell clumping. The cells were moved to −20 °C for 30 min and subsequently stored at −80 °C for long-term storage.

Rehydration of Methanol Fixed Cells. To preserve RNA integrity, it is crucial that all the steps of methanol rehydration were performed at +4 °C. Recovery of cells upon methanol rehydration steps was ∼50%. To obtain the final suspension of 1 × 10^6/mL rehydrated cells, 2 × 10^6 methanol fixed cells were used in each experiment. Cells (2 × 10^6) were spun down at 4500*g* for 5 min in 4 °C precooled centrifuge. The supernatant was removed, and the cells were resuspended in 0.5 mL of resuspension buffer: 3× SSC (Millipore Sigma, S6639−1L), 0.04% BSA (Gibco, 15260037), 1 mM DDT, and 0.2 U/μL RNase Inhibitor (Millipore Sigma, 3335402001) in nuclease-free water. The cells were counted with AO/PI staining on the automated cell counter (Nexcelom, Cellometer Auto 2000). Finally, dilution of cells was brought to ∼1 × 10^6 cells/mL, which was the optimal number for downstream single-cell sequencing analysis.

Sectioning of Organoids. Organoids were fixed in 4% paraformaldehyde (PFA) in 1× PBS for 30 min at room temperature. Further, organoids were immersed in 30% sucrose solutions in 1× PBS and left on a rocking platform overnight at 4 °C. Organoids were embedded in sectioning molds and covered with O.C.T. Compound (Tissue-Tek, 4583) and quickly frozen in ethanol/dry ice bath. Samples were sectioned to 20 μm thickness on the Leica CM3050 S cryostat and collected on glass slides. The samples were then stored at −20 °C until usage.

Immunohistochemistry. Samples were thawed at room temperature for 20 min and then washed in 1× PBS. For staining the nuclear epitopes, an antigen retrieval was performed, except for RBFOX1 nuclear staining (Figure 7), where antigen retrieval was omitted. The antigen retrieval was performed in 1× citrate buffer with pH 6.0 in ddH_2O (Electron Microscopy Sciences, 64142−08). 1 × citrate buffer of pH 6.0 in ddH_2O was warmed up to 95 °C and applied over samples for 20 min and allowed to cool at room temperature. The samples were washed three times with a wash buffer (1 × PBS, 0.1% Tween-20), followed by 30 min of permeabilization (0.3% TritonX-100 in 1 × PBS). The samples were quenched with 0.1 M glycine at 7.4 pH for 20 min, followed by 30 min incubation in a blocking buffer: 5% goat serum (Rockland, D104000050) or 5% normal donkey serum (Millipore Sigma, 566460), 0.1% TritonX-100 in 1× PBS. The primary antibodies were incubated overnight at 4 °C, followed by incubation of secondary antibodies for 2 h in the blocking buffer (see Key Resource Table). After two washes in 1× PBS and one time in ddH_2O, the samples were mounted with a VECTASHIELD Vibrance Mounting Medium (Vector Laboratories, H-1700).

Image Acquisition. Images were acquired with an Opera Phenix (PerkinElmer) high-content confocal imager using a 20× water objective with numerical aperture 1. To set the glass slides, the adapter was used to position the glass slides into the imager. To locate the specimen (hCOs), a 5× objective was used. The images were acquired with Harmony Phenologic (PerkinElmer) software. Each image represents stitched tile scan (41−211 tiles) with 5% overlap, four channels (405, 488, 594, and 647), and 6−8 *z*-planes. For all images, a confocal setting was used.

To stitch the tile scan images (Figure 2F,G), we exported them out of Harmony Phenologic (PerkinElmer) software and imported the whole data sets into ArivisVision4D software. The ArivisVision4D software allows automatic image stitching. Finally, the stitched maximum projections of tiled images were exported as separate.tiff files—4 different channels (405, 488, 594, and 647). Lastly, final contrast settings and merge of 4 channels were done in ImageJ/Fiji software using functions "B&C" and "merge channels".[94] All the images represent a maximum projection of 6−8 *z*-planes, of which each *z*-plane has an optical thickness of 1 μm.

Quantification of Immunofluorescence. To quantify the nuclear immunofluorescence intensity value on high-content confocal images of hCOs, we used "image analysis" mode in Harmony PhenoLOGIC software. On average, we analyzed 3 fixed 20 μm thick and fluorescently labeled cross-sections from 3 independent 90 day old hCOs per cell line (6 controls [CTRL_H9 batch 1 and 2; CTRL_8402 batch 1 2, CTRL_H1, CTRL_1030] and 6 cell lines each from individual hemideletion patients). Prior to quantification, 6−8 *z*-planes (each *z*-plane 2 μm thick) were collapsed into a maximum projection image. We developed a custom-made pipeline that (1) recognizes all nuclei using DAPI staining; (2) distinguishes live and dead (pyknotic) nuclei based on nuclear size and immunofluorescence brightness intensity; (3) determines RBFOX1-positive nuclei; and (4) determines SOX2-positive nuclei. All immunofluorescence signal intensities were kept identical throughout all specimens. Quantifications of selected markers (RBFOX1 and SOX2) (Figures 7C; S7C) were expressed as a percentage of the number of nuclei for the selected marker over the total number of

https://doi.org/10.1021/acschemneuro.3c00442
ACS Chem. Neurosci. 2023, 14, 3993−4012

DAPI-positive live nuclei. Quantification was done on all fields acquired; in total, we measured the intensity on 1096 different fields, containing 1,201,643 live cells out of which 344,217 nuclei were positive for RBFOX1 (~29% out of the total live cells) and 379,280 nuclei were positive for SOX2 (~32% out of total live cells) (Table S6). Intensity of the nuclear immunofluorescence signals for selected markers (RBFOX1 and SOX2) were normalized using average intensity of 6 control cell lines (CTRL_H9 batch 1 and 2; CTRL_8402 batch 1 2, CTRL_H1, CTRL_1030) (Figures 7D and S7C).

Single-Cell RNA-seq Library Generation and Sequencing. Single-cell RNA-seq (scRNA-seq) library construction was performed using the 10X Genomics 3′ Gene Expression kit v3 (cat. #1000075). The rehydrated organoid cells were run through the 10X controller, and subsequent library construction was completed in accordance with the manufacturer's protocol. Library quality was checked using the Bioanalyzer (Agilent Technologies) and sequenced on a NovaSeq 6000 (Illumina). These samples were generated with a target of 4000−6000 cells per sample and 50,000 reads per cell.

scRNA-seq Data Analysis. Primary analysis of the scRNA-seq data was performed using CellRanger (10X Genomics). BCL files were demultiplexed and converted to fastq format using *cellranger mkfastq*, and fastq files were aligned to HG38 using *cellranger count*. All subsequent analyses were performed in R (v 4.0.2), primarily using Seurat v3 (satijalab.org). Count data from each sample were merged, the aggregated data were normalized and scaled, and technical and biological batch effects were regressed using SCTransform (Seurat). single cell double scoring (SCDS)was used to help identify and filter out doublets. Cells with a hybrid score greater than 1.4 were removed from the data set. Dimensionality reduction was performed with principal component analysis (PCA). We determined the *k*-nearest neighbors (KNN) for each cell from this reduction and used the KNN graph to calculate a shared nearest neighbors (SNN) graph. Seurat's *FindClusters* function was used to identify clusters in the data using an SNN modularity optimization-based clustering algorithm. Cells were labeled using human fetal brain scRNA-seq data as a referenceref 47. The fetal brain raw count data was imported and run through the same basic pipeline as our internal data using *SCTransform*, and the original cell type annotations from the authors were used as input for cell type identification in our data set. Seurat's *TransferAnchors* function was used to identify fetal brain cell type signatures in the organoid data set and record each cell's similarity to those signatures with a score (prediction score) from 0 to 1. Organoid cells were annotated as the cell type with which they had the highest prediction score from the fetal brain data. In Figure 1, internal data and human fetal brain data were integrated using Seurat's *IntegrateData* function with the human fetal brain data as the reference data set. RNA velocity analysis was performed using STARsolo (https://github.com/alexdobin/STAR) and velocyto.R (https://github.com/velocyto-team/velocyto.R).

Pseudobulk Differential Expression Analysis. Pseudobulk analysis was performed by using the sum of all cells from a given sample or all the cells from a defined subset of cells from a given sample as input for differential expression using DESeq2 (https://bioconductor.org/packages/release/bioc/html/DESeq2.html).

GO Analyses. Gene set enrichment analyses were performed separately on nine cell types for biological processes (BP) using the clusterProfiler package in R.[95] The full enrichment tables for the down- and upregulated genes are shown as heatmaps, in which the color gradients represent the normalized enrichment scores (NESs) (Figure 6A and Table S4). Next, for an easier interpretation, the enriched GO terms were clustered based on the similarity matrix of their underlying gene sets using the bioconductor package simplifyEnrichment.[96] The resulting 11 clusters were then termed by drawing on the most common words within each cluster.

STATISTICAL ANALYSIS

Statistical analysis was performed either in R (v 4.0.2) using Pearson's Correlation or ANOVA test (Figures 1D, 4A,C, S5A,S5B, and S7B) or in GraphPad Prism (v 9.1.2) using the *t*-test (Figures 7C,D and S7C,D).

ASSOCIATED CONTENT

Data Availability Statement

Raw patient sequencing data will require an MTA from Stanford, Simons Foundation, and NIH. Gene count tables and differential expression, which lack nucleotide resolution or average expression across patients are available (https://sandbox.zenodo.org/record/1103196#.Yxo8EUdBw2w).Code is available via the https://github.com/Novartis/16p11.2-Organoid-scRNA-seq (16p11.2scRNA).

Supporting Information

The Supporting Information is available free of charge at https://pubs.acs.org/doi/10.1021/acschemneuro.3c00442.

Pearson and Spearman correlation values and list of previous publications used for benchmarking (XLSX)

List of cell lines, metadata, karyotyping, and aCGH FISH (XLSX)

List of cell-specific DE genes in CTRL vs DEL and CTRL vs DUP vs DU (XLSX)

List of GO:BP IDs used (XLSX)

Gene−disease network analysis results for downregulated and upregulated genes (XLSX)

Quantification metadata for RBFOX1 and SOX2 percentage and immunofluorescence analysis (XLSX)

List of previously published RBFOX1-dependent genes, DE genes from this study, and overlap of the lists (XLSX)

Quality control of methanol fixation protocol; verification of 16p11.2 hemideletion and hemiduplication in hPSC lines used in this study; scRNA-seq profiling of hCOs derived from 16p11.2 CNV patient lines; volcano plot showing DE genes in patient hemiduplication vs. control lines; cell-type-specific expression of selected genes in hemideletion hCOs; GO analyses; and specificity of RBFOX1 mRNA expression and SOX2 protein expression in 90 day old hCOs (PDF)

AUTHOR INFORMATION

Corresponding Author

Robert J. Ihry − *Neuroscience, Novartis Institutes for BioMedical Research, Cambridge 02139 Massachusetts, United States;* orcid.org/0000-0003-4519-3136; Email: robert.ihry@novartis.com

Authors

Milos Kostic − *Neuroscience, Novartis Institutes for BioMedical Research, Cambridge 02139 Massachusetts, United States*

Joseph J. Raymond − *Neuroscience, Novartis Institutes for BioMedical Research, Cambridge 02139 Massachusetts, United States*

Christophe A. C. Freyre − *Neuroscience, Novartis Institutes for BioMedical Research, Cambridge 02139 Massachusetts, United States;* orcid.org/0000-0001-6775-4665

Beata Henry − *Neuroscience, Novartis Institutes for BioMedical Research, Cambridge 02139 Massachusetts, United States*

Tayfun Tumkaya − *Neuroscience, Novartis Institutes for BioMedical Research, Cambridge 02139 Massachusetts, United States; Chemical Biology and Therapeutics, Novartis*

https://doi.org/10.1021/acschemneuro.3c00442
ACS Chem. Neurosci. 2023, 14, 3993−4012

Institutes for BioMedical Research, Cambridge 02139 Massachusetts, United States

Jivan Khlghatyan − *Neuroscience, Novartis Institutes for BioMedical Research, Cambridge 02139 Massachusetts, United States*

Jill Dvornik − *Neuroscience, Novartis Institutes for BioMedical Research, Cambridge 02139 Massachusetts, United States*

Jingyao Li − *Neuroscience, Novartis Institutes for BioMedical Research, Cambridge 02139 Massachusetts, United States*

Jack S. Hsiao − *Neuroscience, Novartis Institutes for BioMedical Research, Cambridge 02139 Massachusetts, United States*

Seon Hye Cheon − *Neuroscience, Novartis Institutes for BioMedical Research, Cambridge 02139 Massachusetts, United States*

Jonathan Chung − *Chemical Biology and Therapeutics, Novartis Institutes for BioMedical Research, Cambridge 02139 Massachusetts, United States*

Yishan Sun − *Neuroscience, Novartis Institutes for BioMedical Research, Cambridge 02139 Massachusetts, United States*

Ricardo E. Dolmetsch − *Neuroscience, Novartis Institutes for BioMedical Research, Cambridge 02139 Massachusetts, United States*

Kathleen A. Worringer − *Neuroscience, Novartis Institutes for BioMedical Research, Cambridge 02139 Massachusetts, United States*

Complete contact information is available at: https://pubs.acs.org/10.1021/acschemneuro.3c00442

Author Contributions

[§]M.K., J.J.R., K.A.W., and R.J.I. designed experiments and wrote the manuscript. B.H. developed methods to perform automated feeding of organoids. M.K. and Y.S. developed organoid protocols. M.K. optimized methanol fixation and performed IHC analysis. J.J.R. performed and analyzed scRNA-seq data. T.T. and J.C. performed gene set enrichment analysis and genomic analysis. J.K. and J.D. cultured organoids. J.S.H. and S.H.C performed copy number analysis and Q.C. of patient iPSC lines. R.D. acquired and transferred cell lines and arranged the MTAs to support this project. C.F. and J.L. prepared data and code for final submission.

Funding

Research was funded by the Novartis Institutes for BioMedical Reasearch.

Notes

The authors declare the following competing financial interest(s): During the time of this research, all scientists were employed by the Novartis Institutes for BioMedical Research.

■ ACKNOWLEDGMENTS

We are grateful to all the families at the participating Simons Simplex Collection (SSC) sites, as well as the principal investigators at Stanford and NIH who contributed and generated fibroblasts and pluripotent stem cells for this study. We would like to thank Bulent Ataman for thoughtful discussion and feedback on the project.

■ REFERENCES

(1) Bill, B. R.; Lowe, J. K.; DyBuncio, C. T.; Fogel, B. L. Orchestration of Neurodevelopmental Programs by RBFOX1. *Int. Rev. Neurobiol.* **2013**, *113*, 251−267.

(2) Fogel, B. L.; Wexler, E.; Wahnich, A.; Friedrich, T.; Vijayendran, C.; Gao, F.; Parikshak, N.; Konopka, G.; Geschwind, D. H. RBFOX1 Regulates Both Splicing and Transcriptional Networks in Human Neuronal Development. *Hum. Mol. Genet.* **2012**, *21* (19), 4171−4186.

(3) Lal, D.; Reinthaler, E. M.; Altmüller, J.; Toliat, M. R.; Thiele, H.; Nürnberg, P.; Lerche, H.; Hahn, A.; Møller, R. S.; Muhle, H.; Sander, T.; Zimprich, F.; Neubauer, B. A. RBFOX1 and RBFOX3Mutations in Rolandic Epilepsy. *PLoS One* **2013**, *8* (9), No. e73323.

(4) Noor, A.; Lionel, A. C.; Cohen-Woods, S.; Moghimi, N.; Rucker, J.; Fennell, A.; Thiruvahindrapuram, B.; Kaufman, L.; Degagne, B.; Wei, J.; Parikh, S. V.; Muglia, P.; Forte, J.; Scherer, S. W.; Kennedy, J. L.; Xu, W.; McGuffin, P.; Farmer, A.; Strauss, J.; Vincent, J. B. Copy Number Variant Study of Bipolar Disorder in Canadian and UK Populations Implicates Synaptic Genes. *Am. J. Med. Genet.* **2014**, *165* (4), 303−313.

(5) Zarrei, M.; Burton, C. L.; Engchuan, W.; Young, E. J.; Higginbotham, E. J.; MacDonald, J. R.; Trost, B.; Chan, A. J. S.; Walker, S.; Lamoureux, S.; Heung, T.; Mojarad, B. A.; Kellam, B.; Paton, T.; Faheem, M.; Miron, K.; Lu, C.; Wang, T.; Samler, K.; Wang, X.; Costain, G.; Hoang, N.; Pellecchia, G.; Wei, J.; Patel, R. V.; Thiruvahindrapuram, B.; Roifman, M.; Merico, D.; Goodale, T.; Drmic, I.; Speevak, M.; Howe, J. L.; Yuen, R. K. C.; Buchanan, J. A.; Vorstman, J. A. S.; Marshall, C. R.; Wintle, R. F.; Rosenberg, D. R.; Hanna, G. L.; Woodbury-Smith, M.; Cytrynbaum, C.; Zwaigenbaum, L.; Elsabbagh, M.; Flanagan, J.; Fernandez, B. A.; Carter, M. T.; Szatmari, P.; Roberts, W.; Lerch, J.; Liu, X.; Nicolson, R.; Georgiades, S.; Weksberg, R.; Arnold, P. D.; Bassett, A. S.; Crosbie, J.; Schachar, R.; Stavropoulos, D. J.; Anagnostou, E.; Scherer, S. W. A Large Data Resource of Genomic Copy Number Variation across Neurodevelopmental Disorders. *npj Genom. Med.* **2019**, *4* (1), 26.

(6) Kirov, G.; Rees, E.; Walters, J. T. R.; Escott-Price, V.; Georgieva, L.; Richards, A. L.; Chambert, K. D.; Davies, G.; Legge, S. E.; Moran, J. L.; McCarroll, S. A.; O'Donovan, M. C.; Owen, M. J. The Penetrance of Copy Number Variations for Schizophrenia and Developmental Delay. *Biol. Psychiatry* **2014**, *75* (5), 378−385.

(7) Kumar, R. A.; KaraMohamed, S.; Sudi, J.; Conrad, D. F.; Brune, C.; Badner, J. A.; Gilliam, T. C.; Nowak, N. J.; Cook, E. H.; Dobyns, W. B.; Christian, S. L. Recurrent 16p11.2 Microdeletions in Autism. *Hum. Mol. Genet.* **2007**, *17* (4), 628−638.

(8) Fernandez, B. A.; Roberts, W.; Chung, B.; Weksberg, R.; Meyn, S.; Szatmari, P.; Joseph-George, A. M.; MacKay, S.; Whitten, K.; Noble, B.; Vardy, C.; Crosbie, V.; Luscombe, S.; Tucker, E.; Turner, L.; Marshall, C. R.; Scherer, S. W. Phenotypic Spectrum Associated with de Novo and Inherited Deletions and Duplications at 16p11.2 in Individuals Ascertained for Diagnosis of Autism Spectrum Disorder. *J. Med. Genet* **2010**, *47* (3), 195−203.

(9) Rosenfeld, J. A.; Coppinger, J.; Bejjani, B. A.; Girirajan, S.; Eichler, E. E.; Shaffer, L. G.; Ballif, B. C. Speech Delays and Behavioral Problems Are the Predominant Features in Individuals with Developmental Delays and 16p11.2 Microdeletions and Microduplications. *J. Neurodev. Disord.* **2010**, *2* (1), 26−38.

(10) Shinawi, M.; Liu, P.; Kang, S. H. L.; Shen, J.; Belmont, J. W.; Scott, D. A.; Probst, F. J.; Craigen, W. J.; Graham, B. H.; Pursley, A.; Clark, G.; Lee, J.; Proud, M.; Stocco, A.; Rodriguez, D. L.; Kozel, B. A.; Sparagana, S.; Roeder, E. R.; McGrew, S. G.; Kurczynski, T. W.; Allison, L. J.; Amato, S.; Savage, S.; Patel, A.; Stankiewicz, P.; Beaudet, A. L.; Cheung, S. W.; Lupski, J. R. Recurrent Reciprocal 16p11.2 Rearrangements Associated with Global Developmental Delay, Behavioural Problems, Dysmorphism, Epilepsy, and Abnormal Head Size. *J. Med. Genet* **2010**, *47* (5), 332−341.

(11) Hanson, E.; Bernier, R.; Porche, K.; Jackson, F. I.; Goin-Kochel, R. P.; Snyder, L. G.; Snow, A. V.; Wallace, A. S.; Campe, K. L.; Zhang, Y.; Chen, Q.; D'Angelo, D.; Moreno-De-Luca, A.; Orr, P. T.; Boomer, K. B.; Evans, D. W.; Kanne, S.; Berry, L.; Miller, F. K.; Olson, J.; Sherr, E.; Martin, C. L.; Ledbetter, D. H.; Spiro, J. E.; Chung, W. K. The Cognitive and Behavioral Phenotype of the 16p11.2 Deletion in a Clinically Ascertained Population. *Biol. Psychiatry* **2015**, *77* (9), 785−793.

(12) Niarchou, M.; Chawner, S. J. R. A.; Doherty, J. L.; Maillard, A. M.; Jacquemont, S.; Chung, W. K.; Green-Snyder, L.; Bernier, R. A.; Goin-Kochel, R. P.; Hanson, E.; Linden, D. E. J.; Linden, S. C.; Raymond, F. L.; Skuse, D.; Hall, J.; Owen, M. J.; Bree, M. B. M. v. d. Psychiatric Disorders in Children with 16p11.2 Deletion and Duplication. *Transl. Psychiatry* **2019**, *9* (1), 8.
(13) Chawner, S. J. R. A.; Doherty, J. L.; Anney, R. J. L.; Antshel, K. M.; Bearden, C. E.; Bernier, R.; Chung, W. K.; Clements, C. C.; Curran, S. R.; Cuturilo, G.; Fiksinski, A. M.; Gallagher, L.; Goin-Kochel, R. P.; Gur, R. E.; Hanson, E.; Jacquemont, S.; Kates, W. R.; Kushan, L.; Maillard, A. M.; McDonald-McGinn, D. M.; Mihaljevic, M.; Miller, J. S.; Moss, H.; Pejovic-Milovancevic, M.; Schultz, R. T.; Green-Snyder, L.; Vorstman, J. A.; Wenger, T. L.; Hall, J.; Owen, M. J.; van den Bree, M. B. M. A Genetics-First Approach to Dissecting the Heterogeneity of Autism: Phenotypic Comparison of Autism Risk Copy Number Variants. *AJP* **2021**, *178* (1), 77−86.
(14) Fetit, R.; Price, D. J.; Lawrie, S. M.; Johnstone, M. Understanding the Clinical Manifestations of 16p11.2 Deletion Syndrome: A Series of Developmental Case Reports in Children. *Psychiatr. Genet.* **2020**, *30* (5), 136−140.
(15) Loviglio, M. N.; Leleu, M.; Männik, K.; Passeggeri, M.; Giannuzzi, G.; van der Werf, I.; Waszak, S. M.; Zazhytska, M.; Roberts-Caldeira, I.; Gheldof, N.; Migliavacca, E.; Alfaiz, A. A.; Hippolyte, L.; Maillard, A. M.; Van Dijck, A.; Kooy, R. F.; Sanlaville, D.; Rosenfeld, J. A.; Shaffer, L. G.; Andrieux, J.; Marshall, C.; Scherer, S. W.; Shen, Y.; Gusella, J. F.; Thorsteinsdottir, U.; Thorleifsson, G.; Dermitzakis, E. T.; Deplancke, B.; Beckmann, J. S.; Rougemont, J.; Jacquemont, S.; Reymond, A. Chromosomal Contacts Connect Loci Associated with Autism, BMI and Head Circumference Phenotypes. *Mol. Psychiatry* **2017**, *22* (6), 836−849.
(16) Chung, W. K.; Roberts, T. P.; Sherr, E. H.; Snyder, L. G.; Spiro, J. E. 16p11.2 Deletion Syndrome. *Curr. Opin. Genet. Dev.* **2021**, *68*, 49−56.
(17) Weiss, L. A.; Shen, Y.; Korn, J. M.; Arking, D. E.; Miller, D. T.; Fossdal, R.; Saemundsen, E.; Stefansson, H.; Ferreira, M. A. R.; Green, T.; Platt, O. S.; Ruderfer, D. M.; Walsh, C. A.; Altshuler, D.; Chakravarti, A.; Tanzi, R. E.; Stefansson, K.; Santangelo, S. L.; Gusella, J. F.; Sklar, P.; Wu, B.-L.; Daly, M. J. Association between Microdeletion and Microduplication at 16p11.2 and Autism. *N. Engl. J. Med.* **2008**, *358* (7), 667−675.
(18) McCarthy, S. E.; Makarov, V.; Kirov, G.; Addington, A. M.; McClellan, J.; Yoon, S.; Perkins, D. O.; Dickel, D. E.; Kusenda, M.; Krastoshevsky, O.; Krause, V.; Kumar, R. A.; Grozeva, D.; Malhotra, D.; Walsh, T.; Zackai, E. H.; Kaplan, P.; Ganesh, J.; Krantz, I. D.; Spinner, N. B.; Roccanova, P.; Bhandari, A.; Pavon, K.; Lakshmi, B.; Leotta, A.; Kendall, J.; Lee, Y.; Vacic, V.; Gary, S.; Iakoucheva, L. M.; Crow, T. J.; Christian, S. L.; Lieberman, J. A.; Stroup, T. S.; Lehtimäki, T.; Puura, K.; Haldeman-Englert, C.; Pearl, J.; Goodell, M.; Willour, V. L.; DeRosse, P.; Steele, J.; Kassem, L.; Wolff, J.; Chitkara, N.; McMahon, F. J.; Malhotra, A. K.; Potash, J. B.; Schulze, T. G.; Nöthen, M. M.; Cichon, S.; Rietschel, M.; Leibenluft, E.; Kustanovich, V.; Lajonchere, C. M.; Sutcliffe, J. S.; Skuse, D.; Gill, M.; Gallagher, L.; Mendell, N. R.; Craddock, N.; Owen, M. J.; O'Donovan, M. C.; Shaikh, T. H.; Susser, E.; DeLisi, L. E.; Sullivan, P. F.; Deutsch, C. K.; Rapoport, J.; Levy, D. L.; King, M.-C.; Sebat, J. Microduplications of 16p11.2 Are Associated with Schizophrenia. *Nat. Genet.* **2009**, *41* (11), 1223−1227.
(19) Guha, S.; Rees, E.; Darvasi, A.; Ivanov, D.; Ikeda, M.; Bergen, S. E.; Magnusson, P. K.; Cormican, P.; Morris, D.; Gill, M.; Cichon, S.; Rosenfeld, J. A.; Lee, A.; Gregersen, P. K.; Kane, J. M.; Malhotra, A. K.; Rietschel, M.; Nöthen, M. M.; Degenhardt, F.; Priebe, L.; Breuer, R.; Strohmaier, J.; Ruderfer, D. M.; Moran, J. L.; Chambert, K. D.; Sanders, A. R.; Shi, J.; Kendler, K.; Riley, B.; O'Neill, T.; Walsh, D.; Malhotra, D.; Corvin, A.; Purcell, S.; Sklar, P.; Iwata, N.; Hultman, C. M.; Sullivan, P. F.; Sebat, J.; McCarthy, S.; Gejman, P. V.; Levinson, D. F.; Owen, M. J.; O'Donovan, M. C.; Lencz, T.; Kirov, G. Implication of a Rare Deletion at Distal 16p11.2 in Schizophrenia. *JAMA Psychiatry* **2013**, *70* (3), 253−260.
(20) Marshall, C. R.; Howrigan, D. P.; Merico, D.; Thiruvahindrapuram, B.; Wu, W.; Greer, D. S.; Antaki, D.; Shetty, A.; Holmans, P. A.; Pinto, D.; Gujral, M.; Brandler, W. M.; Malhotra, D.; Wang, Z.; Fajarado, K. V. F.; Maile, M. S.; Ripke, S.; Agartz, I.; Albus, M.; Alexander, M.; Amin, F.; Atkins, J.; Bacanu, S. A.; Belliveau, R. A.; Bergen, S. E.; Bertalan, M.; Bevilacqua, E.; Bigdeli, T. B.; Black, D. W.; Bruggeman, R.; Buccola, N. G.; Buckner, R. L.; Bulik-Sullivan, B.; Byerley, W.; Cahn, W.; Cai, G.; Cairns, M. J.; Campion, D.; Cantor, R. M.; Carr, V. J.; Carrera, N.; Catts, S. V.; Chambert, K. D.; Cheng, W.; Cloninger, C. R.; Cohen, D.; Cormican, P.; Craddock, N.; Crespo-Facorro, B.; Crowley, J. J.; Curtis, D.; Davidson, M.; Davis, K. L.; Degenhardt, F.; Del Favero, J.; DeLisi, L. E.; Dikeos, D.; Dinan, T.; Djurovic, S.; Donohoe, G.; Drapeau, E.; Duan, J.; Dudbridge, F.; Eichhammer, P.; Eriksson, J.; Escott-Price, V.; Essioux, L.; Fanous, A. H.; Farh, K.-H.; Farrell, M. S.; Frank, J.; Franke, L.; Freedman, R.; Freimer, N. B.; Friedman, J. I.; Forstner, A. J.; Fromer, M.; Genovese, G.; Georgieva, L.; Gershon, E. S.; Giegling, I.; Giusti-Rodríguez, P.; Godard, S.; Goldstein, J. I.; Gratten, J.; de Haan, L.; Hamshere, M. L.; Hansen, M.; Hansen, T.; Haroutunian, V.; Hartmann, A. M.; Henskens, F. A.; Herms, S.; Hirschhorn, J. N.; Hoffmann, P.; Hofman, A.; Huang, H.; Ikeda, M.; Joa, I.; Kähler, A. K.; Kahn, R. S.; Kalaydjieva, L.; Karjalainen, J.; Kavanagh, D.; Keller, M. C.; Kelly, B. J.; Kennedy, J. L.; Kim, Y.; Knowles, J. A.; Konte, B.; Laurent, C.; Lee, P.; Lee, S. H.; Legge, S. E.; Lerer, B.; Levy, D. L.; Liang, K.-Y.; Lieberman, J.; Lönnqvist, J.; Loughland, C. M.; Magnusson, P. K. E.; Maher, B. S.; Maier, W.; Mallet, J.; Mattheisen, M.; Mattingsdal, M.; McCarley, R. W.; McDonald, C.; McIntosh, A. M.; Meier, S.; Meijer, C. J.; Melle, I.; Mesholam-Gately, R. I.; Metspalu, A.; Michie, P. T.; Milani, L.; Milanova, V.; Mokrab, Y.; Morris, D. W.; Müller-Myhsok, B.; Murphy, K. C.; Murray, R. M.; Myin-Germeys, I.; Nenadic, I.; Nertney, D. A.; Nestadt, G.; Nicodemus, K. K.; Nisenbaum, L.; Nordin, A.; O'Callaghan, E.; O'Dushlaine, C.; Oh, S.-Y.; Olincy, A.; Olsen, L.; O'Neill, F. A.; Van Os, J.; Pantelis, C.; Papadimitriou, G. N.; Parkhomenko, E.; Pato, M. T.; Paunio, T.; Perkins, D. O.; Pers, T. H.; Pietiläinen, O.; Pimm, J.; Pocklington, A. J.; Powell, J.; Price, A.; Pulver, A. E.; Purcell, S. M.; Quested, D.; Rasmussen, H. B.; Reichenberg, A.; Reimers, M. A.; Richards, A. L.; Roffman, J. L.; Roussos, P.; Ruderfer, D. M.; Salomaa, V.; Sanders, A. R.; Savitz, A.; Schall, U.; Schulze, T. G.; Schwab, S. G.; Scolnick, E. M.; Scott, R. J.; Seidman, L. J.; Shi, J.; Silverman, J. M.; Smoller, J. W.; Söderman, E.; Spencer, C. C. A.; Stahl, E. A.; Strengman, E.; Strohmaier, J.; Stroup, T. S.; Suvisaari, J.; Svrakic, D. M.; Szatkiewicz, J. P.; Thirumalai, S.; Tooney, P. A.; Veijola, J.; Visscher, P. M.; Waddington, J.; Walsh, D.; Webb, B. T.; Weiser, M.; Wildenauer, D. B.; Williams, N. M.; Williams, S.; Witt, S. H.; Wolen, A. R.; Wormley, B. K.; Wray, N. R.; Wu, J. Q.; Zai, C. C.; Adolfsson, R.; Andreassen, O. A.; Blackwood, D. H. R.; Bramon, E.; Buxbaum, J. D.; Cichon, S.; Collier, D. A.; Corvin, A.; Daly, M. J.; Darvasi, A.; Domenici, E.; Esko, T.; Gejman, P. V.; Gill, M.; Gurling, H.; Hultman, C. M.; Iwata, N.; Jablensky, A. V.; Jönsson, E. G.; Kendler, K. S.; Kirov, G.; Knight, J.; Levinson, D. F.; Li, Q. S.; McCarroll, S. A.; McQuillin, A.; Moran, J. L.; Mowry, B. J.; Nöthen, M. M.; Ophoff, R. A.; Owen, M. J.; Palotie, A.; Pato, C. N.; Petryshen, T. L.; Posthuma, D.; Rietschel, M.; Riley, B. P.; Rujescu, D.; Sklar, P.; St Clair, D.; Walters, J. T. R.; Werge, T.; Sullivan, P. F.; O'Donovan, M. C.; Scherer, S. W.; Neale, B. M.; Sebat, J. Contribution of Copy Number Variants to Schizophrenia from a Genome-Wide Study of 41,321 Subjects. *Nat. Genet.* **2017**, *49* (1), 27−35.
(21) Chang, Y. S.; Owen, J. P.; Pojman, N. J.; Thieu, T.; Bukshpun, P.; Wakahiro, M. L. J.; Marco, E. J.; Berman, J. I.; Spiro, J. E.; Chung, W. K.; Buckner, R. L.; Roberts, T. P. L.; Nagarajan, S. S.; Sherr, E. H.; Mukherjee, P. Reciprocal White Matter Alterations Due to 16p11.2 Chromosomal Deletions versus Duplications: White Matter Microstructure in 16p11.2 CNVs. *Hum. Brain Mapp.* **2016**, *37* (8), 2833−2848.
(22) Florio, M.; Huttner, W. B. Neural Progenitors, Neurogenesis and the Evolution of the Neocortex. *Development* **2014**, *141* (11), 2182−2194.

https://doi.org/10.1021/acschemneuro.3c00442
ACS Chem. Neurosci. 2023, 14, 3993−4012

(23) Nuttle, X.; Giannuzzi, G.; Duyzend, M. H.; Schraiber, J. G.; Narvaiza, I.; Sudmant, P. H.; Penn, O.; Chiatante, G.; Malig, M.; Huddleston, J.; Benner, C.; Camponeschi, F.; Ciofi-Baffoni, S.; Stessman, H. A. F.; Marchetto, M. C. N.; Denman, L.; Harshman, L.; Baker, C.; Raja, A.; Penewit, K.; Janke, N.; Tang, W. J.; Ventura, M.; Banci, L.; Antonacci, F.; Akey, J. M.; Amemiya, C. T.; Gage, F. H.; Reymond, A.; Eichler, E. E. Emergence of a Homo Sapiens-Specific Gene Family and Chromosome 16p11.2 CNV Susceptibility. *Nature* **2016**, *536* (7615), 205−209.
(24) Arbogast, T.; Ouagazzal, A.-M.; Chevalier, C.; Kopanitsa, M.; Afinowi, N.; Migliavacca, E.; Cowling, B. S.; Birling, M.-C.; Champy, M.-F.; Reymond, A.; Herault, Y. Reciprocal Effects on Neurocognitive and Metabolic Phenotypes in Mouse Models of 16p11.2 Deletion and Duplication Syndromes. *PLoS Genet.* **2016**, *12* (2), No. e1005709.
(25) Portmann, T.; Yang, M.; Mao, R.; Panagiotakos, G.; Ellegood, J.; Dolen, G.; Bader, P. L.; Grueter, B. A.; Goold, C.; Fisher, E.; Clifford, K.; Rengarajan, P.; Kalikhman, D.; Loureiro, D.; Saw, N. L.; Zhengqui, Z.; Miller, M. A.; Lerch, J. P.; Henkelman, R. M.; Shamloo, M.; Malenka, R. C.; Crawley, J. N.; Dolmetsch, R. E. Behavioral Abnormalities and Circuit Defects in the Basal Ganglia of a Mouse Model of 16p11.2 Deletion Syndrome. *Cell Rep.* **2014**, *7* (4), 1077−1092.
(26) Takahashi, K.; Yamanaka, S. Induction of Pluripotent Stem Cells from Mouse Embryonic and Adult Fibroblast Cultures by Defined Factors. *Cell* **2006**, *126* (4), 663−676.
(27) Takahashi, K.; Tanabe, K.; Ohnuki, M.; Narita, M.; Ichisaka, T.; Tomoda, K.; Yamanaka, S. Induction of Pluripotent Stem Cells from Adult Human Fibroblasts by Defined Factors. *Cell* **2007**, *131* (5), 861−872.
(28) Zhang, Y.; Pak, C.; Han, Y.; Ahlenius, H.; Zhang, Z.; Chanda, S.; Marro, S.; Patzke, C.; Acuna, C.; Covy, J.; Xu, W.; Yang, N.; Danko, T.; Chen, L.; Wernig, M.; Südhof, T. Rapid Single-Step Induction of Functional Neurons from Human Pluripotent Stem Cells. *Neuron* **2013**, *78* (5), 785−798.
(29) Chambers, S. M.; Fasano, C. A.; Papapetrou, E. P.; Tomishima, M.; Sadelain, M.; Studer, L. Highly Efficient Neural Conversion of Human ES and IPS Cells by Dual Inhibition of SMAD Signaling. *Nat. Biotechnol.* **2009**, *27* (3), 275−280.
(30) Shi, Y.; Kirwan, P.; Smith, J.; Robinson, H. P. C.; Livesey, F. J. Human Cerebral Cortex Development from Pluripotent Stem Cells to Functional Excitatory Synapses. *Nat. Neurosci.* **2012**, *15* (3), 477−486.
(31) Deshpande, A.; Yadav, S.; Dao, D. Q.; Wu, Z.-Y.; Hokanson, K. C.; Cahill, M. K.; Wiita, A. P.; Jan, Y.-N.; Ullian, E. M.; Weiss, L. A. Cellular Phenotypes in Human IPSC-Derived Neurons from a Genetic Model of Autism Spectrum Disorder. *Cell Rep.* **2017**, *21* (10), 2678−2687.
(32) Roth, J. G.; Muench, K. L.; Asokan, A.; Mallett, V. M.; Gai, H.; Verma, Y.; Weber, S.; Charlton, C.; Fowler, J. L.; Loh, K. M.; Dolmetsch, R. E.; Palmer, T. D. 16p11.2 Microdeletion Imparts Transcriptional Alterations in Human IPSC-Derived Models of Early Neural Development. *eLife* **2020**, *9*, No. e58178.
(33) Lancaster, M. A.; Renner, M.; Martin, C.-A.; Wenzel, D.; Bicknell, L. S.; Hurles, M. E.; Homfray, T.; Penninger, J. M.; Jackson, A. P.; Knoblich, J. A. Cerebral Organoids Model Human Brain Development and Microcephaly. *Nature* **2013**, *501* (7467), 373−379.
(34) Mariani, J.; Coppola, G.; Zhang, P.; Abyzov, A.; Provini, L.; Tomasini, L.; Amenduni, M.; Szekely, A.; Palejev, D.; Wilson, M.; Gerstein, M.; Grigorenko, E. L.; Chawarska, K.; Pelphrey, K. A.; Howe, J. R.; Vaccarino, F. M. FOXG1-Dependent Dysregulation of GABA/Glutamate Neuron Differentiation in Autism Spectrum Disorders. *Cell* **2015**, *162* (2), 375−390.
(35) Qian, X.; Nguyen, H. N.; Song, M. M.; Hadiono, C.; Ogden, S. C.; Hammack, C.; Yao, B.; Hamersky, G. R.; Jacob, F.; Zhong, C.; Yoon, K.; Jeang, W.; Lin, L.; Li, Y.; Thakor, J.; Berg, D. A.; Zhang, C.; Kang, E.; Chickering, M.; Nauen, D.; Ho, C.-Y.; Wen, Z.; Christian, K. M.; Shi, P.-Y.; Maher, B. J.; Wu, H.; Jin, P.; Tang, H.; Song, H.; Ming, G. Brain-Region-Specific Organoids Using Mini-Bioreactors for Modeling ZIKV Exposure. *Cell* **2016**, *165* (5), 1238−1254.
(36) Birey, F.; Andersen, J.; Makinson, C. D.; Islam, S.; Wei, W.; Huber, N.; Fan, H. C.; Metzler, K. R. C.; Panagiotakos, G.; Thom, N.; O'Rourke, N. A.; Steinmetz, L. M.; Bernstein, J. A.; Hallmayer, J.; Huguenard, J. R.; Paşca, S. P. Assembly of Functionally Integrated Human Forebrain Spheroids. *Nature* **2017**, *545* (7652), 54−59.
(37) Trujillo, C. A.; Gao, R.; Negraes, P. D.; Gu, J.; Buchanan, J.; Preissl, S.; Wang, A.; Wu, W.; Haddad, G. G.; Chaim, I. A.; Domissy, A.; Vandenberghe, M.; Devor, A.; Yeo, G. W.; Voytek, B.; Muotri, A. R. Complex Oscillatory Waves Emerging from Cortical Organoids Model Early Human Brain Network Development. *Cell Stem Cell* **2019**, *25* (4), 558−569.e7.
(38) Macosko, E. Z.; Basu, A.; Satija, R.; Nemesh, J.; Shekhar, K.; Goldman, M.; Tirosh, I.; Bialas, A. R.; Kamitaki, N.; Martersteck, E. M.; Trombetta, J. J.; Weitz, D. A.; Sanes, J. R.; Shalek, A. K.; Regev, A.; McCarroll, S. A. Highly Parallel Genome-Wide Expression Profiling of Individual Cells Using Nanoliter Droplets. *Cell* **2015**, *161* (5), 1202−1214.
(39) Camp, J. G.; Badsha, F.; Florio, M.; Kanton, S.; Gerber, T.; Wilsch-Bräuninger, M.; Lewitus, E.; Sykes, A.; Hevers, W.; Lancaster, M.; Knoblich, J. A.; Lachmann, R.; Pääbo, S.; Huttner, W. B.; Treutlein, B. Human Cerebral Organoids Recapitulate Gene Expression Programs of Fetal Neocortex Development. *Proc. Natl. Acad. Sci. U.S.A.* **2015**, *112* (51), 15672−15677.
(40) Quadrato, G.; Nguyen, T.; Macosko, E. Z.; Sherwood, J. L.; Min Yang, S.; Berger, D. R.; Maria, N.; Scholvin, J.; Goldman, M.; Kinney, J. P.; Boyden, E. S.; Lichtman, J. W.; Williams, Z. M.; McCarroll, S. A.; Arlotta, P. Cell Diversity and Network Dynamics in Photosensitive Human Brain Organoids. *Nature* **2017**, *545* (7652), 48−53.
(41) Velasco, S.; Kedaigle, A. J.; Simmons, S. K.; Nash, A.; Rocha, M.; Quadrato, G.; Paulsen, B.; Nguyen, L.; Adiconis, X.; Regev, A.; Levin, J. Z.; Arlotta, P. Individual Brain Organoids Reproducibly Form Cell Diversity of the Human Cerebral Cortex. *Nature* **2019**, *570* (7762), 523−527.
(42) Bhaduri, A.; Andrews, M. G.; Mancia Leon, W.; Jung, D.; Shin, D.; Allen, D.; Jung, D.; Schmunk, G.; Haeussler, M.; Salma, J.; Pollen, A. A.; Nowakowski, T. J.; Kriegstein, A. R. Cell Stress in Cortical Organoids Impairs Molecular Subtype Specification. *Nature* **2020**, *578* (7793), 142−148.
(43) Paşca, A. M.; Sloan, S. A.; Clarke, L. E.; Tian, Y.; Makinson, C. D.; Huber, N.; Kim, C. H.; Park, J.-Y.; O'Rourke, N. A.; Nguyen, K. D.; Smith, S. J.; Huguenard, J. R.; Geschwind, D. H.; Barres, B. A.; Paşca, S. P. Functional Cortical Neurons and Astrocytes from Human Pluripotent Stem Cells in 3D Culture. *Nat. Methods* **2015**, *12* (7), 671−678.
(44) Chen, J.; Cheung, F.; Shi, R.; Zhou, H.; Lu, W. PBMC Fixation and Processing for Chromium Single-Cell RNA Sequencing. *J. Transl. Med.* **2018**, *16* (1), 198.
(45) Zheng, G. X. Y.; Terry, J. M.; Belgrader, P.; Ryvkin, P.; Bent, Z. W.; Wilson, R.; Ziraldo, S. B.; Wheeler, T. D.; McDermott, G. P.; Zhu, J.; Gregory, M. T.; Shuga, J.; Montesclaros, L.; Underwood, J. G.; Masquelier, D. A.; Nishimura, S. Y.; Schnall-Levin, M.; Wyatt, P. W.; Hindson, C. M.; Bharadwaj, R.; Wong, A.; Ness, K. D.; Beppu, L. W.; Deeg, H. J.; McFarland, C.; Loeb, K. R.; Valente, W. J.; Ericson, N. G.; Stevens, E. A.; Radich, J. P.; Mikkelsen, T. S.; Hindson, B. J.; Bielas, J. H. Massively Parallel Digital Transcriptional Profiling of Single Cells. *Nat. Commun.* **2017**, *8* (1), 14049.
(46) Butler, A.; Hoffman, P.; Smibert, P.; Papalexi, E.; Satija, R. Integrating Single-Cell Transcriptomic Data across Different Conditions, Technologies, and Species. *Nat. Biotechnol.* **2018**, *36* (5), 411−420.
(47) Luecken, M. D.; Theis, F. J. Current Best Practices in Single-Cell RNA-Seq Analysis: A Tutorial. *Mol. Syst. Biol.* **2019**, *15* (6), No. e8746.
(48) Polioudakis, D.; de la Torre-Ubieta, L.; Langerman, J.; Elkins, A. G.; Shi, X.; Stein, J. L.; Vuong, C. K.; Nichterwitz, S.; Gevorgian, M.; Opland, C. K.; Lu, D.; Connell, W.; Ruzzo, E. K.; Lowe, J. K.; Hadzic, T.; Hinz, F. I.; Sabri, S.; Lowry, W. E.; Gerstein, M. B.; Plath, K.; Geschwind, D. H. A Single-Cell Transcriptomic Atlas of Human

https://doi.org/10.1021/acschemneuro.3c00442
ACS Chem. Neurosci. 2023, 14, 3993−4012

Neocortical Development during Mid-Gestation. *Neuron* **2019**, *103* (5), 785−801.e8.
(49) La Manno, G.; Soldatov, R.; Zeisel, A.; Braun, E.; Hochgerner, H.; Petukhov, V.; Lidschreiber, K.; Kastriti, M. E.; Lönnerberg, P.; Furlan, A.; Fan, J.; Borm, L. E.; Liu, Z.; van Bruggen, D.; Guo, J.; He, X.; Barker, R.; Sundström, E.; Castelo-Branco, G.; Cramer, P.; Adameyko, I.; Linnarsson, S.; Kharchenko, P. V. RNA Velocity of Single Cells. *Nature* **2018**, *560* (7719), 494−498.
(50) Haubensak, W.; Attardo, A.; Denk, W.; Huttner, W. B. Neurons Arise in the Basal Neuroepithelium of the Early Mammalian Telencephalon: A Major Site of Neurogenesis. *6. Biol. Sci.* **2004**, *101* (9), 3196−3201.
(51) Miyata, T.; Kawaguchi, A.; Saito, K.; Kawano, M.; Muto, T.; Ogawa, M. Asymmetric Production of Surface-Dividing and Non-Surface-Dividing Cortical Progenitor Cells. *Development* **2004**, *131* (13), 3133−3145.
(52) Noctor, S. C.; Martínez-Cerdeño, V.; Ivic, L.; Kriegstein, A. R. Cortical Neurons Arise in Symmetric and Asymmetric Division Zones and Migrate through Specific Phases. *Nat. Neurosci.* **2004**, *7* (2), 136−144.
(53) Shitamukai, A.; Matsuzaki, F. Control of Asymmetric Cell Division of Mammalian Neural Progenitors. *Dev., Growth Differ.* **2012**, *54* (3), 277−286.
(54) Eze, U. C.; Bhaduri, A.; Haeussler, M.; Nowakowski, T. J.; Kriegstein, A. R. Single-Cell Atlas of Early Human Brain Development Highlights Heterogeneity of Human Neuroepithelial Cells and Early Radial Glia. *Nat. Neurosci.* **2020**, *24*, 584.
(55) Hansen, D. V.; Lui, J. H.; Parker, P. R. L.; Kriegstein, A. R. Neurogenic Radial Glia in the Outer Subventricular Zone of Human Neocortex. *Nature* **2010**, *464* (7288), 554−561.
(56) Fietz, S. A.; Kelava, I.; Vogt, J.; Wilsch-Bräuninger, M.; Stenzel, D.; Fish, J. L.; Corbeil, D.; Riehn, A.; Distler, W.; Nitsch, R.; Huttner, W. B. OSVZ Progenitors of Human and Ferret Neocortex Are Epithelial-like and Expand by Integrin Signaling. *Nat. Neurosci.* **2010**, *13* (6), 690−699.
(57) Nowakowski, T. J.; Pollen, A. A.; Di Lullo, E.; Sandoval-Espinosa, C.; Bershteyn, M.; Kriegstein, A. R. Expression Analysis Highlights AXL as a Candidate Zika Virus Entry Receptor in Neural Stem Cells. *Cell Stem Cell* **2016**, *18* (5), 591−596.
(58) Greig, L. C.; Woodworth, M. B.; Galazo, M. J.; Padmanabhan, H.; Macklis, J. D. Molecular Logic of Neocortical Projection Neuron Specification, Development and Diversity. *Nat. Rev. Neurosci.* **2013**, *14* (11), 755−769.
(59) Molyneaux, B. J.; Arlotta, P.; Menezes, J. R. L.; Macklis, J. D. Neuronal Subtype Specification in the Cerebral Cortex. *Nat. Rev. Neurosci.* **2007**, *8* (6), 427−437.
(60) Eiraku, M.; Watanabe, K.; Matsuo-Takasaki, M.; Kawada, M.; Yonemura, S.; Matsumura, M.; Wataya, T.; Nishiyama, A.; Muguruma, K.; Sasai, Y. Self-Organized Formation of Polarized Cortical Tissues from ESCs and Its Active Manipulation by Extrinsic Signals. *Cell Stem Cell* **2008**, *3* (5), 519−532.
(61) van den Ameele, J.; Tiberi, L.; Vanderhaeghen, P.; Espuny-Camacho, I. Thinking out of the Dish: What to Learn about Cortical Development Using Pluripotent Stem Cells. *Trends Neurosci.* **2014**, *37* (6), 334−342.
(62) Tanaka, Y.; Cakir, B.; Xiang, Y.; Sullivan, G. J.; Park, I.-H. Synthetic Analyses of Single-Cell Transcriptomes from Multiple Brain Organoids and Fetal Brain. *Cell Rep.* **2020**, *30* (6), 1682−1689.e3.
(63) Stuart, T.; Butler, A.; Hoffman, P.; Hafemeister, C.; Papalexi, E.; Mauck, W. M.; Hao, Y.; Stoeckius, M.; Smibert, P.; Satija, R. Comprehensive Integration of Single-Cell Data. *Cell* **2019**, *177* (7), 1888−1902.e21.
(64) Rosenfeld, J. A.; Coe, B. P.; Eichler, E. E.; Cuckle, H.; Shaffer, L. G. Estimates of Penetrance for Recurrent Pathogenic Copy-Number Variations. *Genet. Med.* **2013**, *15* (6), 478−481.
(65) Sundberg, M.; Pinson, H.; Smith, R. S.; Winden, K. D.; Venugopal, P.; Tai, D. J. C.; Gusella, J. F.; Talkowski, M. E.; Walsh, C. A.; Tegmark, M.; Sahin, M. 16p11.2 Deletion Is Associated with Hyperactivation of Human IPSC-Derived Dopaminergic Neuron Networks and Is Rescued by RHOA Inhibition in Vitro. *Nat. Commun.* **2021**, *12* (1), 2897.
(66) Luo, R.; Sanders, S. J.; Tian, Y.; Voineagu, I.; Huang, N.; Chu, S. H.; Klei, L.; Cai, C.; Ou, J.; Lowe, J. K.; Hurles, M. E.; Devlin, B.; State, M. W.; Geschwind, D. H. Genome-Wide Transcriptome Profiling Reveals the Functional Impact of Rare De Novo and Recurrent CNVs in Autism Spectrum Disorders. *Am. J. Hum. Genet.* **2012**, *91* (1), 38−55.
(67) Horev, G.; Ellegood, J.; Lerch, J. P.; Son, Y.-E. E.; Muthuswamy, L.; Vogel, H.; Krieger, A. M.; Buja, A.; Henkelman, R. M.; Wigler, M.; Mills, A. A. Dosage-Dependent Phenotypes in Models of 16p11.2 Lesions Found in Autism. *Proc. Natl. Acad. Sci. U.S.A.* **2011**, *108* (41), 17076−17081.
(68) Liao, C.; Fu, F.; Li, R.; Yang, W.; Liao, H.; Yan, J.; Li, J.; Li, S.; Yang, X.; Li, D. Loss-of-Function Variation in the DPP6 Gene Is Associated with Autosomal Dominant Microcephaly and Mental Retardation. *Eur. J. Med. Genet.* **2013**, *56* (9), 484−489.
(69) Neale, B. M.; Medland, S.; Ripke, S.; Anney, R. J. L.; Asherson, P.; Buitelaar, J.; Franke, B.; Gill, M.; Kent, L.; Holmans, P.; Middleton, F.; Thapar, A.; Lesch, K.-P.; Faraone, S. V.; Daly, M.; Nguyen, T. T.; Schäfer, H.; Steinhausen, H.-C.; Reif, A.; Renner, T. J.; Romanos, M.; Romanos, J.; Warnke, A.; Walitza, S.; Freitag, C.; Meyer, J.; Palmason, H.; Rothenberger, A.; Hawi, Z.; Sergeant, J.; Roeyers, H.; Mick, E.; Biederman, J. Case-Control Genome-Wide Association Study of Attention-Deficit/Hyperactivity Disorder. *J. Am. Acad. Child Adolesc. Psychiatry* **2010**, *49* (9), 906−920.
(70) Hamada, N.; Ito, H.; Nishijo, T.; Iwamoto, I.; Morishita, R.; Tabata, H.; Momiyama, T.; Nagata, K.-I. Essential Role of the Nuclear Isoform of RBFOX1, a Candidate Gene for Autism Spectrum Disorders, in the Brain Development. *Sci. Rep.* **2016**, *6* (1), 30805.
(71) Südhof, T. C. Neuroligins and Neurexins Link Synaptic Function to Cognitive Disease. *Nature* **2008**, *455* (7215), 903−911.
(72) Gandawijaya, J.; Bamford, R. A.; Burbach, J. P. H.; Oguro-Ando, A. Cell Adhesion Molecules Involved in Neurodevelopmental Pathways Implicated in 3p-Deletion Syndrome and Autism Spectrum Disorder. *Front. Cell. Neurosci.* **2021**, *14*, 611379.
(73) Chen, J. A.; Peñagarikano, O.; Belgard, T. G.; Swarup, V.; Geschwind, D. H. The Emerging Picture of Autism Spectrum Disorder: Genetics and Pathology. *Annu. Rev. Pathol. Mech. Dis.* **2015**, *10* (1), 111−144.
(74) Lee, P. H.; Anttila, V.; Won, H.; Feng, Y.-C. A.; Rosenthal, J.; Zhu, Z.; Tucker-Drob, E. M.; Nivard, M. G.; Grotzinger, A. D.; Posthuma, D.; Wang, M. M.-J.; Yu, D.; Stahl, E. A.; Walters, R. K.; Anney, R. J. L.; Duncan, L. E.; Ge, T.; Adolfsson, R.; Banaschewski, T.; Belangero, S.; Cook, E. H.; Coppola, G.; Derks, E. M.; Hoekstra, P. J.; Kaprio, J.; Keski-Rahkonen, A.; Kirov, G.; Kranzler, H. R.; Luykx, J. J.; Rohde, L. A.; Zai, C. C.; Agerbo, E.; Arranz, M. J.; Asherson, P.; Bækvad-Hansen, M.; Baldursson, G.; Bellgrove, M.; Belliveau, R. A.; Buitelaar, J.; Burton, C. L.; Bybjerg-Grauholm, J.; Casas, M.; Cerrato, F.; Chambert, K.; Churchhouse, C.; Cormand, B.; Crosbie, J.; Dalsgaard, S.; Demontis, D.; Doyle, A. E.; Dumont, A.; Elia, J.; Grove, J.; Gudmundsson, O. O.; Haavik, J.; Hakonarson, H.; Hansen, C. S.; Hartman, C. A.; Hawi, Z.; Hervás, A.; Hougaard, D. M.; Howrigan, D. P.; Huang, H.; Kuntsi, J.; Langley, K.; Lesch, K.-P.; Leung, P. W. L.; Loo, S. K.; Martin, J.; Martin, A. R.; McGough, J. J.; Medland, S. E.; Moran, J. L.; Mors, O.; Mortensen, P. B.; Oades, R. D.; Palmer, D. S.; Pedersen, C. B.; Pedersen, M. G.; Peters, T.; Poterba, T.; Poulsen, J. B.; Ramos-Quiroga, J. A.; Reif, A.; Ribasés, M.; Rothenberger, A.; Rovira, P.; Sánchez-Mora, C.; Satterstrom, F. K.; Schachar, R.; Artigas, M. S.; Steinberg, S.; Stefansson, H.; Turley, P.; Walters, G. B.; Werge, T.; Zayats, T.; Arking, D. E.; Bettella, F.; Buxbaum, J. D.; Christensen, J. H.; Collins, R. L.; Coon, H.; De Rubeis, S.; Delorme, R.; Grice, D. E.; Hansen, T. F.; Holmans, P. A.; Hope, S.; Hultman, C. M.; Klei, L.; Ladd-Acosta, C.; Magnusson, P.; Nærland, T.; Nyegaard, M.; Pinto, D.; Qvist, P.; Rehnström, K.; Reichenberg, A.; Reichert, J.; Roeder, K.; Rouleau, G. A.; Saemundsen, E.; Sanders, S. J.; Sandin, S.; St Pourcain, B.; Stefansson, K.; Sutcliffe, J. S.; Talkowski, M. E.; Weiss, L. A.; Willsey, A. J.; Agartz, I.; Akil, H.; Albani, D.; Alda, M.; Als, T. D.;

https://doi.org/10.1021/acschemneuro.3c00442
ACS Chem. Neurosci. 2023, 14, 3993−4012

Anjorin, A.; Backlund, L.; Bass, N.; Bauer, M.; Baune, B. T.; Bellivier, F.; Bergen, S. E.; Berrettini, W. H.; Biernacka, J. M.; Blackwood, D. H. R.; Bøen, E.; Budde, M.; Bunney, W.; Burmeister, M.; Byerley, W.; Byrne, E. M.; Cichon, S.; Clarke, T.-K.; Coleman, J. R. I.; Craddock, N.; Curtis, D.; Czerski, P. M.; Dale, A. M.; Dalkner, N.; Dannlowski, U.; Degenhardt, F.; Di Florio, A.; Elvsåshagen, T.; Etain, B.; Fischer, S. B.; Forstner, A. J.; Forty, L.; Frank, J.; Frye, M.; Fullerton, J. M.; Gade, K.; Gaspar, H. A.; Gershon, E. S.; Gill, M.; Goes, F. S.; Gordon, S. D.; Gordon-Smith, K.; Green, M. J.; Greenwood, T. A.; Grigoroiu-Serbanescu, M.; Guzman-Parra, J.; Hauser, J.; Hautzinger, M.; Heilbronner, U.; Herms, S.; Hoffmann, P.; Holland, D.; Jamain, S.; Jones, I.; Jones, L. A.; Kandaswamy, R.; Kelsoe, J. R.; Kennedy, J. L.; Joachim, O. K.; Kittel-Schneider, S.; Kogevinas, M.; Koller, A. C.; Lavebratt, C.; Lewis, C. M.; Li, Q. S.; Lissowska, J.; Loohuis, L. M. O.; Lucae, S.; Maaser, A.; Malt, U. F.; Martin, N. G.; Martinsson, L.; McElroy, S. L.; McMahon, F. J.; McQuillin, A.; Melle, I.; Metspalu, A.; Millischer, V.; Mitchell, P. B.; Montgomery, G. W.; Morken, G.; Morris, D. W.; Müller-Myhsok, B.; Mullins, N.; Myers, R. M.; Nievergelt, C. M.; Nordentoft, M.; Adolfsson, A. N.; Nöthen, M. M.; Ophoff, R. A.; Owen, M. J.; Paciga, S. A.; Pato, C. N.; Pato, M. T.; Perlis, R. H.; Perry, A.; Potash, J. B.; Reinbold, C. S.; Rietschel, M.; Rivera, M.; Roberson, M.; Schalling, M.; Schofield, P. R.; Schulze, T. G.; Scott, L. J.; Serretti, A.; Sigurdsson, E.; Smeland, O. B.; Stordal, E.; Streit, F.; Strohmaier, J.; Thorgeirsson, T. E.; Treutlein, J.; Turecki, G.; Vaaler, A. E.; Vieta, E.; Vincent, J. B.; Wang, Y.; Witt, S. H.; Zandi, P.; Adan, R. A. H.; Alfredsson, L.; Ando, T.; Aschauer, H.; Baker, J. H.; Bencko, V.; Bergen, A. W.; Birgegård, A.; Perica, V. B.; Brandt, H.; Burghardt, R.; Carlberg, L.; Cassina, M.; Clementi, M.; Courtet, P.; Crawford, S.; Crow, S.; Crowley, J. J.; Danner, U. N.; Davis, O. S. P.; Degortes, D.; DeSocio, J. E.; Dick, D. M.; Dina, C.; Docampo, E.; Egberts, K.; Ehrlich, S.; Espeseth, T.; Fernández-Aranda, F.; Fichter, M. M.; Foretova, L.; Forzan, M.; Gambaro, G.; Giegling, I.; Gonidakis, F.; Gorwood, P.; Mayora, M. G.; Guo, Y.; Halmi, K. A.; Hatzikotoulas, K.; Hebebrand, J.; Helder, S. G.; Herpertz-Dahlmann, B.; Herzog, W.; Hinney, A.; Imgart, H.; Jiménez-Murcia, S.; Johnson, C.; Jordan, J.; Julià, A.; Kaminská, D.; Karhunen, L.; Karwautz, A.; Kas, M. J. H.; Kaye, W. H.; Kennedy, M. A.; Kim, Y.-R.; Klareskog, L.; Klump, K. L.; Knudsen, G. P. S.; Landén, M.; Le Hellard, S.; Levitan, R. D.; Li, D.; Lichtenstein, P.; Maj, M.; Marsal, S.; McDevitt, S.; Mitchell, J.; Monteleone, P.; Monteleone, A. M.; Munn-Chernoff, M. A.; Nacmias, B.; Navratilova, M.; O'Toole, J. K.; Padyukov, L.; Pantel, J.; Papezova, H.; Rabionet, R.; Raevuori, A.; Ramoz, N.; Reichborn-Kjennerud, T.; Ricca, V.; Roberts, M.; Rujescu, D.; Rybakowski, F.; Scherag, A.; Schmidt, U.; Seitz, J.; Slachtova, L.; Slof-Op't Landt, M. C. T.; Slopien, A.; Sorbi, S.; Southam, L.; Strober, M.; Tortorella, A.; Tozzi, F.; Treasure, J.; Tziouvas, K.; van Elburg, A. A.; Wade, T. D.; Wagner, G.; Walton, E.; Watson, H. J.; Wichmann, H.-E.; Woodside, D. B.; Zeggini, E.; Zerwas, S.; Zipfel, S.; Adams, M. J.; Andlauer, T. F. M.; Berger, K.; Binder, E. B.; Boomsma, D. I.; Castelao, E.; Colodro-Conde, L.; Direk, N.; Docherty, A. R.; Domenici, E.; Domschke, K.; Dunn, E. C.; Foo, J. C.; de Geus, E. J. C.; Grabe, H. J.; Hamilton, S. P.; Horn, C.; Hottenga, J.-J.; Howard, D.; Ising, M.; Kloiber, S.; Levinson, D. F.; Lewis, G.; Magnusson, P. K. E.; Mbarek, H.; Middeldorp, C. M.; Mostafavi, S.; Nyholt, D. R.; Penninx, B. W. J. H.; Peterson, R. E.; Pistis, G.; Porteous, D. J.; Preisig, M.; Quiroz, J. A.; Schaefer, C.; Schulte, E. C.; Shi, J.; Smith, D. J.; Thomson, P. A.; Tiemeier, H.; Uher, R.; van der Auwera, S.; Weissman, M. M.; Alexander, M.; Begemann, M.; Bramon, E.; Buccola, N. G.; Cairns, M. J.; Campion, D.; Carr, V. J.; Cloninger, C. R.; Cohen, D.; Collier, D. A.; Corvin, A.; DeLisi, L. E.; Donohoe, G.; Dudbridge, F.; Duan, J.; Freedman, R.; Gejman, P. V.; Golimbet, V.; Godard, S.; Ehrenreich, H.; Hartmann, A. M.; Henskens, F. A.; Ikeda, M.; Iwata, N.; Jablensky, A. V.; Joa, I.; Jönsson, E. G.; Kelly, B. J.; Knight, J.; Konte, B.; Laurent-Levinson, C.; Lee, J.; Lencz, T.; Lerer, B.; Loughland, C. M.; Malhotra, A. K.; Mallet, J.; McDonald, C.; Mitjans, M.; Mowry, B. J.; Murphy, K. C.; Murray, R. M.; O'Neill, F. A.; Oh, S.-Y.; Palotie, A.; Pantelis, C.; Pulver, A. E.; Petryshen, T. L.; Quested, D. J.; Riley, B.; Sanders, A. R.; Schall, U.; Schwab, S. G.; Scott, R. J.; Sham, P. C.; Silverman, J. M.; Sim, K.; Steixner, A. A.; Tooney, P. A.; van Os, J.; Vawter, M. P.; Walsh, D.; Weiser, M.; Wildenauer, D. B.; Williams, N. M.; Wormley, B. K.; Zhang, F.; Androutsos, C.; Arnold, P. D.; Barr, C. L.; Barta, C.; Bey, K.; Bienvenu, O. J.; Black, D. W.; Brown, L. W.; Budman, C.; Cath, D.; Cheon, K.-A.; Ciullo, V.; Coffey, B. J.; Cusi, D.; Davis, L. K.; Denys, D.; Depienne, C.; Dietrich, A.; Eapen, V.; Falkai, P.; Fernandez, T. V.; Garcia-Delgar, B.; Geller, D. A.; Gilbert, D. L.; Grados, M. A.; Greenberg, E.; Grünblatt, E.; Hagstrøm, J.; Hanna, G. L.; Hartmann, A.; Hedderly, T.; Heiman, G. A.; Heyman, I.; Hong, H. J.; Huang, A.; Huyser, C.; Ibanez-Gomez, L.; Khramtsova, E. A.; Kim, Y. K.; Kim, Y.-S.; King, R. A.; Koh, Y.-J.; Konstantinidis, A.; Kook, S.; Kuperman, S.; Leventhal, B. L.; Lochner, C.; Ludolph, A. G.; Madruga-Garrido, M.; Malaty, I.; Maras, A.; McCracken, J. T.; Meijer, I. A.; Mir, P.; Morer, A.; Müller-Vahl, K. R.; Münchau, A.; Murphy, T. L.; Naarden, A.; Nagy, P.; Nestadt, G.; Nestadt, P. S.; Nicolini, H.; Nurmi, E. L.; Okun, M. S.; Paschou, P.; Piras, F.; Piras, F.; Pittenger, C.; Plessen, K. J.; Richter, M. A.; Rizzo, R.; Robertson, M.; Roessner, V.; Ruhrmann, S.; Samuels, J. F.; Sandor, P.; Schlögelhofer, M.; Shin, E.-Y.; Singer, H.; Song, D.-H.; Song, J.; Spalletta, G.; Stein, D. J.; Stewart, S. E.; Storch, E. A.; Stranger, B.; Stuhrmann, M.; Tarnok, Z.; Tischfield, J. A.; Tübing, J.; Visscher, F.; Vulink, N.; Wagner, M.; Walitza, S.; Wanderer, S.; Woods, M.; Worbe, Y.; Zai, G.; Zinner, S. H.; Sullivan, P. F.; Franke, B.; Daly, M. J.; Bulik, C. M.; Lewis, C. M.; McIntosh, A. M.; O'Donovan, M. C.; Zheutlin, A.; Andreassen, O. A.; Børglum, A. D.; Breen, G.; Edenberg, H. J.; Fanous, A. H.; Faraone, S. V.; Gelernter, J.; Mathews, C. A.; Mattheisen, M.; Mitchell, K. S.; Neale, M. C.; Nurnberger, J. I.; Ripke, S.; Santangelo, S. L.; Scharf, J. M.; Stein, M. B.; Thornton, L. M.; Walters, J. T. R.; Wray, N. R.; Geschwind, D. H.; Neale, B. M.; Kendler, K. S.; Smoller, J. W. Genomic Relationships, Novel Loci, and Pleiotropic Mechanisms across Eight Psychiatric Disorders. *Cell* **2019**, *179* (7), 1469−1482.e11.

(75) Costain, G.; Lionel, A. C.; Merico, D.; Forsythe, P.; Russell, K.; Lowther, C.; Yuen, T.; Husted, J.; Stavropoulos, D. J.; Speevak, M.; Chow, E. W. C.; Marshall, C. R.; Scherer, S. W.; Bassett, A. S. Pathogenic Rare Copy Number Variants in Community-Based Schizophrenia Suggest a Potential Role for Clinical Microarrays. *Hum. Mol. Genet.* **2013**, *22* (22), 4485−4501.

(76) Palumbo, O.; Fischetto, R.; Palumbo, P.; Nicastro, F.; Papadia, F.; Zelante, L.; Carella, M. De Novo Microduplication of CHL1 in a Patient with Non-Syndromic Developmental Phenotypes. *Mol. Cytogenet.* **2015**, *8* (1), 66.

(77) Hu, J.; Liao, J.; Sathanoori, M.; Kochmar, S.; Sebastian, J.; Yatsenko, S. A.; Surti, U. CNTN6 Copy Number Variations in 14 Patients: A Possible Candidate Gene for Neurodevelopmental and Neuropsychiatric Disorders. *J. Neurodev. Disord.* **2015**, *7* (1), 26.

(78) Clelland, C. L.; Drouet, V.; Rilett, K. C.; Smeed, J. A.; Nadrich, R. H.; Rajparia, A.; Read, L. L.; Clelland, J. D. Evidence That COMT Genotype and Proline Interact on Negative-Symptom Outcomes in Schizophrenia and Bipolar Disorder. *Transl. Psychiatry* **2016**, *6* (9), No. e891.

(79) Kuleshov, M. V.; Jones, M. R.; Rouillard, A. D.; Fernandez, N. F.; Duan, Q.; Wang, Z.; Koplev, S.; Jenkins, S. L.; Jagodnik, K. M.; Lachmann, A.; McDermott, M. G.; Monteiro, C. D.; Gundersen, G. W.; Ma'ayan, A. Enrichr: A Comprehensive Gene Set Enrichment Analysis Web Server 2016 Update. *Nucleic Acids Res.* **2016**, *44* (W1), W90−W97.

(80) Chen, E. Y.; Tan, C. M.; Kou, Y.; Duan, Q.; Wang, Z.; Meirelles, G.; Clark, N. R.; Ma'ayan, A. Enrichr: Interactive and Collaborative HTML5 Gene List Enrichment Analysis Tool. *BMC Bioinf.* **2013**, *14* (1), 128.

(81) Xie, Z.; Bailey, A.; Kuleshov, M. V.; Clarke, D. J. B.; Evangelista, J. E.; Jenkins, S. L.; Lachmann, A.; Wojciechowicz, M. L.; Kropiwnicki, E.; Jagodnik, K. M.; et al. Gene Set Knowledge Discovery with Enrichr. *Curr. Protoc.* **2021**, *1* (3), No. e90.

(82) Urresti, J.; Zhang, P.; Moran-Losada, P.; Yu, N.-K.; Negraes, P. D.; Trujillo, C. A.; Antaki, D.; Amar, M.; Chau, K.; Pramod, A. B.; Diedrich, J.; Tejwani, L.; Romero, S.; Sebat, J.; Yates III, J. R.; Muotri, A. R.; Iakoucheva, L. M. Cortical Organoids Model Early Brain

https://doi.org/10.1021/acschemneuro.3c00442
ACS Chem. Neurosci. 2023, 14, 3993−4012

Development Disrupted by 16p11.2 Copy Number Variants in Autism. *Mol. Psychiatry* **2021**, *26* (12), 7560−7580.
(83) Piñero, J.; Ramírez-Anguita, J. M.; Saüch-Pitarch, J.; Ronzano, F.; Centeno, E.; Sanz, F.; Furlong, L. I. The DisGeNET Knowledge Platform for Disease Genomics: 2019 Update. *Nucleic Acids Res.* **2020**, *48*, D845.
(84) Shannon, P.; Markiel, A.; Ozier, O.; Baliga, N. S.; Wang, J. T.; Ramage, D.; Amin, N.; Schwikowski, B.; Ideker, T. Cytoscape: A Software Environment for Integrated Models of Biomolecular Interaction Networks. *Genome Res.* **2003**, *13* (11), 2498−2504.
(85) Rein, B.; Yan, Z. 16p11.2 Copy Number Variations and Neurodevelopmental Disorders. *Trends Neurosci.* **2020**, *43* (11), 886−901.
(86) Nakanishi, M.; Nomura, J.; Ji, X.; Tamada, K.; Arai, T.; Takahashi, E.; Bućan, M.; Takumi, T. Functional Significance of Rare Neuroligin 1 Variants Found in Autism. *PLoS Genet.* **2017**, *13* (8), No. e1006940.
(87) Li, C.; Liu, C.; Zhou, B.; Hu, C.; Xu, X. Novel Micro-duplication of CHL1 Gene in a Patient with Autism Spectrum Disorder: A Case Report and a Brief Literature Review. *Mol. Cytogenet.* **2016**, *9* (1), 51.
(88) Işık, Ü.; Kılıç, F.; Demirdaş, A.; Aktepe, E.; Avşar, P. A. a. Serum Galectin-3 Levels in Children with Attention-Deficit/Hyperactivity Disorder. *Psychiatry Invest.* **2020**, *17* (3), 256−261.
(89) Rademacher, S.; Eickholt, B. J. PTEN in Autism and Neurodevelopmental Disorders. *Cold Spring Harbor Perspect. Med.* **2019**, *9* (11), a036780.
(90) Specchio, N.; Pietrafusa, N.; Trivisano, M.; Moavero, R.; De Palma, L.; Ferretti, A.; Vigevano, F.; Curatolo, P. Autism and Epilepsy in Patients With Tuberous Sclerosis Complex. *Front. Neurol.* **2020**, *11*, 639.
(91) Benítez-Burraco, A.; Barcos-Martínez, M.; Espejo-Portero, I.; Fernández-Urquiza, M.; Torres-Ruiz, R.; Rodríguez-Perales, S.; Jiménez-Romero, M. S. Narrowing the Genetic Causes of Language Dysfunction in the 1q21.1 Microduplication Syndrome. *Front. Pediatr.* **2018**, *6*, 163.
(92) Weiner, D. J.; Ling, E.; Erdin, S.; Tai, D. J. C.; Yadav, R.; Grove, J.; Fu, J. M.; Nadig, A.; Carey, C. E.; Baya, N.; Bybjerg-Grauholm, J.; Mortensen, P. B.; Werge, T.; Demontis, D.; Mors, O.; Nordentoft, M.; Als, T. D.; Baekvad-Hansen, M.; Rosengren, A.; Havdahl, A.; Hedemand, A.; Palotie, A.; Chakravarti, A.; Arking, D.; Sulovari, A.; Starnawska, A.; Thiruvahindrapuram, B.; de Leeuw, C.; Carey, C.; Ladd-Acosta, C.; van der Merwe, C.; Devlin, B.; Cook, E. H.; Eichler, E.; Corfield, E.; Dieleman, G.; Schellenberg, G.; Hakonarson, H.; Coon, H.; Dziobek, I.; Vorstman, J.; Girault, J.; Sutcliffe, J. S.; Duan, J.; Nurnberger, J.; Hallmayer, J.; Buxbaum, J.; Piven, J.; Weiss, L.; Davis, L.; Janecka, M.; Mattheisen, M.; State, M. W.; Gill, M.; Daly, M.; Uddin, M.; Andreassen, O.; Szatmari, P.; Lee, P. H.; Anney, R.; Ripke, S.; Satterstrom, K.; Santangelo, S.; Kuo, S.; van Elst, L. T.; Rolland, T.; Bougeron, T.; Polderman, T.; Turner, T.; Underwood, J.; Manikandan, V.; Pillalamarri, V.; Warrier, V.; Philipsen, A.; Reif, A.; Hinney, A.; Cormand, B.; Bau, C. H. D.; Rovaris, D. L.; Sonuga-Barke, E.; Corfield, E.; Grevet, E. H.; Salum, G.; Larsson, H.; Buitelaar, J.; Haavik, J.; McGough, J.; Kuntsi, J.; Elia, J.; Lesch, K.-P.; Klein, M.; Bellgrove, M.; Tesli, M.; Leung, P. W. L.; Pan, P. M.; Dalsgaard, S.; Loo, S.; Medland, S.; Faraone, S. V.; Reichborn-Kjennerud, T.; Banaschewski, T.; Hawi, Z.; Berretta, S.; Macosko, E. Z.; Sebat, J.; O'Connor, L. J.; Hougaard, D. M.; Børglum, A. D.; Talkowski, M. E.; McCarroll, S. A.; Robinson, E. B. Statistical and functional convergence of common and rare genetic influences on autism at chromosome 16p. *Nat. Genet.* **2022**, *54* (11), 1630−1639.
(93) Tai, D. J. C.; Razaz, P.; Erdin, S.; Gao, D.; Wang, J.; Nuttle, X.; de Esch, C. E.; Collins, R. L.; Currall, B. B.; O'Keefe, K.; Burt, N. D.; Yadav, R.; Wang, L.; Mohajeri, K.; Aneichyk, T.; Ragavendran, A.; Stortchevoi, A.; Morini, E.; Ma, W.; Lucente, D.; Hastie, A.; Kelleher, R. J.; Perlis, R. H.; Talkowski, M. E.; Gusella, J. F. Tissue- and Cell-Type-Specific Molecular and Functional Signatures of 16p11.2 Reciprocal Genomic Disorder across Mouse Brain and Human Neuronal Models. *Am. J. Hum. Genet.* **2022**, *109* (10), 1789−1813.
(94) Schindelin, J.; Arganda-Carreras, I.; Frise, E.; Kaynig, V.; Longair, M.; Pietzsch, T.; Preibisch, S.; Rueden, C.; Saalfeld, S.; Schmid, B.; Tinevez, J.-Y.; White, D. J.; Hartenstein, V.; Eliceiri, K.; Tomancak, P.; Cardona, A. Fiji: An Open-Source Platform for Biological-Image Analysis. *Nat. Methods* **2012**, *9* (7), 676−682.
(95) Yu, G.; Wang, L.-G.; Han, Y.; He, Q.-Y. ClusterProfiler: An R Package for Comparing Biological Themes Among Gene Clusters. *OMICS: J. Integr. Biol.* **2012**, *16* (5), 284−287.
(96) Gu, Z.; Hübschmann, D. SimplifyEnrichment: A Bioconductor Package for Clustering and Visualizing Functional Enrichment Results. *Genomics, Proteomics Bioinf.* **2023**, *21* (1), 190−202.

https://doi.org/10.1021/acschemneuro.3c00442
ACS Chem. Neurosci. 2023, 14, 3993−4012